

WL-TR-94-2100

FUNDAMENTAL STUDIES IN CRYOGENIC
COOLING OF POWER ELECTRONICS



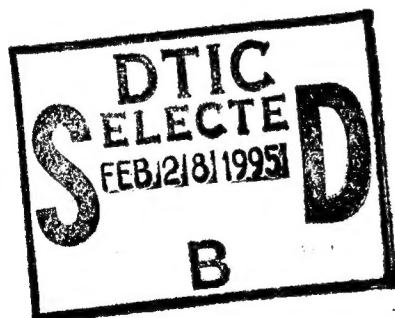
L C CHOW, M S SEHMBEY,
O J HAHM, C J CHUI

UNIVERSITY OF KENTUCKY
DEPARTMENT OF MECHANICAL ENGINEERING
LEXINGTON KY 40506-0046

SEPTEMBER 1994

INTERIM REPORT FOR 09/01/93-08/01/94

APPROVED FOR PUBLIC RELEASE; DISTRIBUTION IS UNLIMITED.



19950217 128


AEROPROPULSION AND POWER DIRECTORATE
WRIGHT LABORATORY
AIR FORCE MATERIEL COMMAND
WRIGHT PATTERSON AFB OH 45433-7251

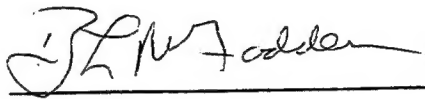
NOTICE


When Government drawings, specifications, or other data are used for any purpose other than in connection with a definitely Government-related procurement, the United States Government incurs no responsibility or any obligation whatsoever. The fact that the government may have formulated or in any way supplied the said drawings, specifications, or other data, is not to be regarded by implication, or otherwise in any manner construed, as licensing the holder, or any other person or corporation; or as conveying any rights or permission to manufacture, use, or sell any patented invention that may in any way be related thereto.

This report is releasable to the National Technical Information Service (NTIS). At NTIS, it will be available to the general public, including foreign nations.

This technical report has been reviewed and is approved for publication.


JEFFREY R. BROWN
Project Engineer
Thermal Technology Section


B. L. MCFADDEN
Chief
Power Technology Branch


MICHAEL D. BRAYDICH, Lt Col, USAF
Deputy Chief
Aerospace Power Division

If your address has changed, if you wish to be removed from our mailing list, or if the addressee is no longer employed by your organization please notify WL/POOS-3, WPAFB, OH 45433-7251 to help us maintain a current mailing list.

Copies of this report should not be returned unless return is required by security considerations, contractual obligations, or notice on a specific document.

REPORT DOCUMENTATION PAGE

Form Approved

OMB No. 0704-0188

Public reporting burden for this collection of information is estimated to average 1 hour per response, including the time for reviewing instructions, searching existing data sources, gathering and maintaining the data needed, and completing and reviewing the collection of information. Send comments regarding this burden estimate or any other aspect of this collection of information, including suggestions for reducing this burden, to Washington Headquarters Services, Directorate for Information Operations and Reports, 1215 Jefferson Davis Highway, Suite 1204, Arlington, VA 22202-4302, and to the Office of Management and Budget, Paperwork Reduction Project (0704-0188), Washington, DC 20503.

1. AGENCY USE ONLY (Leave blank)		2. REPORT DATE 30 Sep 94		3. REPORT TYPE AND DATES COVERED Interim 09/01/93-08/01/94	
4. TITLE AND SUBTITLE Fundamental Studies in Cryogenic Cooling of Power Electronics				5. FUNDING NUMBERS C F33615-91-C-2152 PE 63218 PR 1601 TA 05 WU 03	
6. AUTHOR(S) L.C. Chow O.J. Hahn				M.S. Sehmbe C.J. Chui	
7. PERFORMING ORGANIZATION NAME(S) AND ADDRESS(ES) University of Kentucky Department of Mechanical Engineering Lexington, KY 40506-0046				8. PERFORMING ORGANIZATION REPORT NUMBER UK-ME-94-01	
9. SPONSORING/MONITORING AGENCY NAME(S) AND ADDRESS(ES) Aeropropulsion and Power Directorate Wright Laboratory Air Force Materiel Command Wright Patterson AFB, OH 45433-7251				10. SPONSORING/MONITORING AGENCY REPORT NUMBER WL-TR-94-2100	
11. SUPPLEMENTARY NOTES					
12a. DISTRIBUTION/AVAILABILITY STATEMENT Approved for public release; distribution is unlimited				12b. DISTRIBUTION CODE	
13. ABSTRACT (Maximum 200 words) This study details the results from experiments conducted to study the heat transfer characteristics during liquid nitrogen spray cooling and pool boiling from a heater array. Four different nozzles at various pressures were used to study the variation in spray cooling heat transfer at liquid nitrogen temperature. Effect of nozzle and flow rate on the critical heat flux and the heat transfer coefficient are presented. This study also provides empirical correlations for the spray cooling characteristics. The critical heat flux and the heat transfer coefficient have been correlated using nondimensional numbers. The study also shows the importance of surface roughness for spray cooling with liquid nitrogen. The rougher surfaces were shown to have significantly higher heat transfer rates and similar critical heat fluxes occurring at lower temperatures. The results from experiments conducted to study the pool boiling heat transfer from a vertical array with flush mounted heat sources are also presented. The lower heaters were found to enhance the heat transfer from the upper heaters due to bubble pumped convection.					
14. SUBJECT TERMS Spray Cooling, Pool Boiling, Electronic Cooling, Cryogenics, Liquid Nitrogen				15. NUMBER OF PAGES 65	
				16. PRICE CODE	
17. SECURITY CLASSIFICATION OF REPORT UNCLASSIFIED	18. SECURITY CLASSIFICATION OF THIS PAGE UNCLASSIFIED	19. SECURITY CLASSIFICATION OF ABSTRACT UNCLASSIFIED	20. LIMITATION OF ABSTRACT UL		

DTIC QUALITY INSPECTED 4

TABLE OF CONTENTS

SECTION	PAGE
1. INTRODUCTION	1
2. OBJECTIVES	2
3. BACKGROUND	3
3.1 Superconducting Circuits	3
3.2 Superconductor/Semiconductor Hybrid Circuits	3
3.3 Thermal Management Issues	4
4. SPRAY COOLING WITH LIQUID NITROGEN	8
4.1 Experimental Set-Up	8
4.2 Experimental Procedure	11
4.3 Uncertainty Analysis	13
4.4 Results and Discussion	14
4.5 Data Reduction and Correlation Development	25
4.5.1 Critical Heat Flux	25
4.5.2 Heat Flux	29
5. POOL BOILING FROM A VERTICAL ARRAY IN LIQUID NITROGEN	33
5.1 Experimental Set-Up and Procedure	35
5.2 Uncertainty Analysis	39
5.3 Results and Discussion	41
6. CONCLUSIONS AND FUTURE PLANS	50
7. REFERENCES	52

LIST OF ILLUSTRATIONS

FIGURE	PAGE
3.1 Low Temperature Cooling Scenarios	5
4.1 Spray Cooling Experimental Set-Up	9
4.2 Heater Design	10
4.3 Spray Cooling Characteristics of Different Nozzles	16
4.4 Spray Cooling Physics	17
4.5 Effect of Surface Roughness	20
4.6 CHF versus Mass Flow Rate for Different Nozzles	23
4.7 CHF Dependence on Velocity	24
4.8 CHF Correlation Comparison	26
4.9 Heat Flux Dependence on Reynolds Number	28
4.10 Spray Cooling Heat Flux Correlation	30
5.1 Heater Array Configuration	34
5.2 Heater Construction	36
5.3 Schematic of the Experimental Set-Up	37
5.4 Effect of Lower Heater on Heat Transfer from an Upper Heater	40
5.5 Effect of Lower Heater on Preboiling h	42
5.6 Preboiling h Correlation	45
5.7 Effect of Lower Heater on CHF	46
5.8 CHF Correlation Comparison	48

LIST OF TABLES

TABLE	PAGE
4.1 Nozzle Size	13
4.2 Spray Parameters	15

Accession For	
NTIS GRA&I	<input checked="" type="checkbox"/>
DTIC TAB	<input type="checkbox"/>
Unannounced	<input type="checkbox"/>
Justification	
By	
Distribution	
Availability Codes	
Dist	Avail and/or Special
A-1	

NOMENCLATURE

C_f	heat capacity of the fluid
D	hydraulic diameter of heater surface
d	Sauter mean diameter of spray
G	mass flow rate per unit surface area
g	gravitational acceleration
H_c	distance from center of heater surface to the top of the lower heater
h	heat transfer coefficient, $q''/(T_w - T_{sat})$
h_{fg}	latent heat of evaporation
k_f	thermal conductivity of liquid
L	vertical length of the heater
L_c	length to center of heater ($L/2$)
\dot{m}_f	liquid mass flow rate
Nu_c	Nusselt number at center, hL_c/k_f
$Nu_{n,c}$	natural convection Nusselt number
$Nu_{f,c}$	forced convection Nusselt number
ΔP_f	pressure drop across nozzle exit
q''	heat flux
q''_c	critical heat flux
q''_{lh}	heat flux from lower heater
Ra^*_c	modified Rayleigh number, $C_f \rho^2 g \beta L_c^4 q'' / \mu_f k_f^2$
Re_D	Reynolds number, $\rho_f v D / \mu_f$
Re_{Lc}	Reynolds number, $\rho_f v_f L_c / \mu_f$
T_w	heater surface temperature
T_{sat}	saturation temperature
V	volume flow rate per unit area of heater

v	spray velocity
v_f	liquid velocity
W	heater width
W_1	width of the lower heater
We_D	Weber number based on D , $\rho_f v^2 D / \sigma$
We_L	Weber number, $\rho_f L v_f^2 / \sigma$
β	volume expansion coefficient
μ_0	fluid viscosity at bulk fluid temperature
μ_h	fluid viscosity at mean film temperature
ρ_f	fluid density
ρ_g	vapor density
σ	surface tension

All units in SI unless stated otherwise in text.

1. INTRODUCTION

The future of superconducting and low temperature MOS (metal-oxide semiconductor) electronics holds a great deal of promise. In some cases, the reductions in device sizes and the increased efficiency for liquid nitrogen temperature (LNT) operation may outweigh the cost. The most immediate applications will be in situations where a cryogenic liquid is readily available. In that case, the cryogen can be used as the heat transfer fluid and the size and weight of the onboard electronics can be reduced by an order of magnitude. However, the successful application of cryogenic cooling to electronics requires that the appropriate heat transfer characteristics be known. This is the main objective of this study.

The primary thermal management techniques for low temperature operation are: spray cooling, pool boiling (immersion cooling), forced convection boiling, and jet impingement cooling. This study focusses on spray cooling and pool boiling. Spray cooling was chosen as the first area of research because of its capability in removing large quantities of heat at very low liquid flow rates. Experiments were conducted for various spray cooling conditions using liquid nitrogen. The results of the experiments and the resulting correlations are presented. Pool boiling is the other heat transfer technique which is of great interest due to its simplicity. However, there are some concerns regarding the application of pool boiling in electronic devices containing multiple heat sources. Also, in order to design compact devices, it is important to know the space limitations of the pool boiling technique. Thus, the latter part of this study deals with the behavior of multiple heater arrays in liquid nitrogen and the influence of a confined space.

2. OBJECTIVES

The overall objective of this study is to obtain information on the heat transfer characteristics under conditions of cryogenic cooling in various modes. Also, the suitability of these heat transfer modes to aerospace applications has to be evaluated. Due to the lack of suitable design correlations/models, experimental studies have to be undertaken to evaluate the heat transfer characteristics of liquid nitrogen under: pool boiling in complex geometries, spray cooling, forced convection boiling, and jet impingement. This would be followed by the development of design correlations for these modes of cooling. Finally, the applicability of these techniques to electronic cooling has to be demonstrated.

3. BACKGROUND

The electronic systems envisaged for operation at LNT fall into two categories. First, the superconducting circuits composed of HTS devices (switches, capacitors, inductors, etc.), and second, the hybrid circuits which contain both HTS and semiconductor devices. There are numerous applications for both types of circuits. These two configurations and their applications are discussed in the following sections.

3.1 Superconducting Circuits

Superconducting circuits will consist of HTS devices (logic gates, inverters, memory cells, etc.) with superconducting interconnects [1]. Almost all of the functions performed in high performance electronics can be done by a superconductor circuit [2]. However, superconductor circuits cannot handle high power levels; also, there are no superconducting rectifiers, and semiconductors make better amplifiers and mass memory devices. The main applications of HTS circuits will be

- High speed digital logic and memory: gate speeds under 10 ps are easily achievable using Josephson junctions [1-2] thus allowing the development of faster supercomputers;
- Far infrared/high frequency radar detection: with circuits employing Josephson junction device mixers, very-low-noise high-frequency detection (over 100 GHz) is possible with the only limitation being the Heisenberg uncertainty principle [1,3,4];
- Magnetic field sensors: very sensitive magnetometers and voltmeters made using SQUIDs (superconducting quantum interference devices) have application in magnetic field geophysical exploration and biomagnetic studies of the human body; and
- Superconducting-coil magnets and motors: superconducting-brushless-ac motors can be used in various applications.

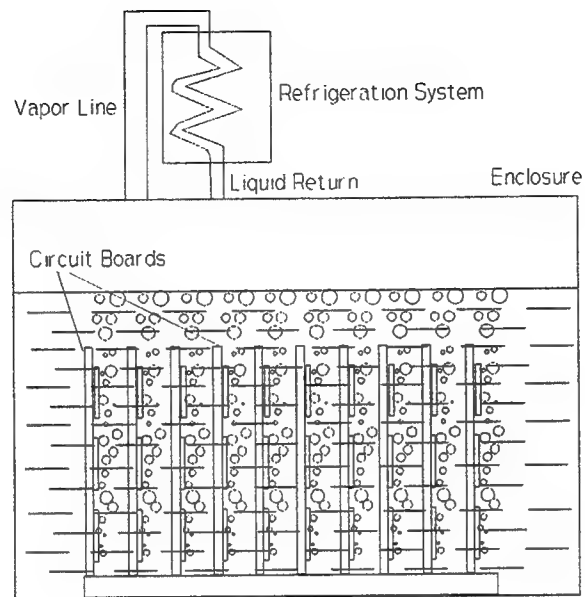
3.2 Superconductor/Semiconductor Hybrid Circuits

MOS semiconductor devices show a marked improvement in performance as the

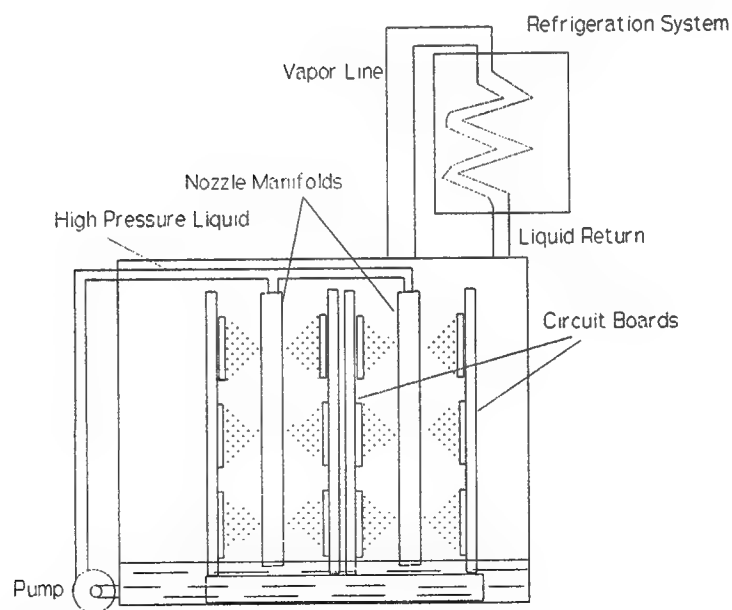
operating temperature is lowered [2,5,6]. Furthermore, the thermal conductivities of semiconductor substrates and packaging materials (silicon, germanium, beryllium, alumina) are seen to increase dramatically as the temperature is lowered to LNT [7]. The main advantages of low temperature operation are: increased electron and hole mobilities, lowered interconnection resistivities, reduced leakage currents, greater subthreshold slope, and reduction in thermal noise. One of the possible applications of low temperature electronics will be in the area of high efficiency ac/dc, dc/ac and RF power conversion at the multikilowatt level. As mentioned earlier, superconducting circuits are not capable of handling high power levels. Hence, MOS field effect transistors (MOSFETs) can be used in combination with high Q inductors and capacitors made from HTSs to obtain the zero voltage switching circuits suitable for power conversion applications [6]. Such an integration will result in a drastic size and weight reduction. The efficiency of these circuits improves greatly at low temperatures due to the dramatic reduction in the on-resistance of power MOSFETs. However, the efficiency of these circuits depends greatly on the Q values of the inductors and capacitors used in the circuit. Hence, it is necessary to use HTSs for these components to obtain the maximum efficiency. Another application of hybrid circuits is the high-frequency receiver-signal processor [2]. Here, the devices best suited for each component of the circuit are used. Thus, a combination of superconductor and semiconductor devices provides a high performance circuit. In industry and transportation, the HTS ac motors employing MOSFET controllers have variety of applications. The HTS-ac motors have been successfully tested recently and will be commercially available in the near future [8]. At the same time, locomotive engines using natural gas (stored at 110 K in liquid form) have been developed [9]. These two can be combined, with the liquefied natural gas acting as the coolant for the HTS motor and MOSFET switches, to produce a highly efficient and clean locomotive engine.

3.3 Thermal Management Issues

A cursory examination of heat transfer requirements in superconducting circuits may lead one to believe that due to the very nature of superconductivity heat dissipation would not be a problem. However, a closer examination reveals how ill-founded that notion is. The main components in a superconducting circuit are the high-speed low-power switches, the Josephson junctions (also called Superconductor-Insulator-Superconductor devices, SISs) [2,4,10]. The main



Immersion (Pool Boiling) Cooling



Spray Cooling System

Figure 3.1 Low Temperature Cooling Scenarios.

advantages of these devices are the low gate delay times and low power dissipation; these features in combination will allow much higher device packing density compared to semiconductor circuits. However, the thermal management aspect of superconducting circuits at LNT has been of concern lately. A typical SIS working at 4.2 K has a power dissipation of 50 kW/m², however, for operation at 77 K, the same device may have a heat dissipation approaching 6000 kW/m² [11]. Obviously, this level of heat dissipation cannot be handled by common heat removal techniques. Hence, there are two options available for the thermal management of HTS circuits:

1. Immersion cooling (pool boiling) in LN2 with low device density packaging employing heat spreaders; and
2. High heat flux cooling with LN2.

The first option cannot be expected to handle device heat dissipation above 500 kW/m². This is because the pool boiling critical heat flux for LN2 is only about 160 kW/m² (calculated using Zuber model [12]). Hence, even with good heat spreaders, the overall device dissipation could not be expected to be more than 2-3 times this amount. Thus, immersion cooling will mean larger, and thereby slower, devices. This may not be a concern in some applications. However, for high speed digital applications, device sizes have to be kept as small as possible in order to minimize the distance travelled by the signal. In those cases the second option of using a high heat flux cooling technique would be much more preferable.

A superconductor/semiconductor hybrid circuits is inherently more prone to thermal failure due to the presence of high heat dissipation transistors in the vicinity of superconducting elements. It is not possible to thermally isolate the superconductor and semiconductor elements because the interconnections themselves serve as thermal bridges. The successful operation of a hybrid circuits depends on the ability of the cooling system to maintain the superconducting elements below their transition temperature. Hence, it is essential that the cooling system is capable of removing high heat fluxes from discrete locations (MOSFETs) to prevent any hot spots and the resultant system failure. Again, in this case, the choices are similar to the ones mentioned before.

Thus, the thermal management scenario in low temperature electronics consists of either using direct immersion pool boiling with heat spreaders, or, a high heat flux cooling technique. For the high heat flux situation, spray cooling is the technique which is of most interest because

of its low liquid flow rate requirements. Low temperature spray cooling consists of subjecting the heat sources with a high speed spray of low temperature liquid. The two thermal management scenarios described above are shown in Figure 3.1. As shown in the figure, both scenarios require a refrigerator/condenser unless the low temperature liquid is available in abundance (as in the case of stored liquefied fuel). The spray cooling scenario will also require a pump for cases where a high pressure liquid is unavailable.

The main concern regarding these techniques is the lack of information about the heat transfer characteristics of cryogenics under the particular conditions described above. Liquid nitrogen was selected as the cryogen for the heat transfer studies due to its suitability for both HTS and MOS devices. The heat transfer characteristics of spray cooling with LN₂ were not available. Also, no general correlations are available for spray cooling. Thus, the spray cooling part of this study dealt with determining the heat transfer characteristics and obtaining suitable correlations. In case of pool boiling, the available correlations deal with simple situations only (e.g., single heater in an unconfined pool of LN₂). However, the conditions in electronic cooling are far more complex due to the interaction of various heaters and lack of space. Thus, the pool boiling part of the study dealt with the effects of multiple heat sources and confined space. The particulars of the experimental studies are presented in the following chapters.

4. SPRAY COOLING WITH LIQUID NITROGEN

Most of the early spray cooling research involved low heat fluxes and low fluid flow rates [13,14]. In the past few years a significant amount of work has been done in high heat flux spray cooling research [15-20]. The complexity of the phenomena involved, have however, frustrated attempts to successfully model the process. Also, the effect of various spray parameters on the heat transfer characteristics is difficult to differentiate because most spray parameters are related to each other. For example, for a particular nozzle, an increase in nozzle pressure causes an increase in spray velocity and mass flow rate, and, a decrease in the mean droplet diameter [21]. Since, the spray cooling heat transfer process is not well understood, the correlations offered by previous researchers are applicable only under the specific conditions of that study. A comprehensive predictive correlation/model for spray cooling is still not available.

Hence, the main objective of this study is to obtain the heat transfer characteristics of spray cooling with liquid nitrogen. This is done by experimentally obtaining heat transfer data for LN2 spray cooling under different spray conditions. The following sections describe the experimental set-up, procedure, results, and data reduction.

4.1 Experiment Set-up

The schematic diagram of the set-up is shown in Figure 4.1. The experimental chamber contains the heater, nozzle, and view ports. The high pressure LN2 dewar is used to supply liquid nitrogen to the nozzle. A heat exchanger between the dewar and the nozzle is used to subcool the high pressure liquid down to about 78 K. Since the chamber is always maintained at atmospheric pressure, the liquid spraying out of the nozzle is always close to saturation if the upstream temperature is maintained at about 78 K (assuming isentropic expansion). All the lines were insulated with polyurethane foam to minimize heat gain. During preliminary experiments, it was found that, at low flow rates, it was very difficult to maintain a single phase fluid supply into the nozzle inlet, this resulted in violent pressure fluctuations and eventual disruption of flow. This happened because the heat gain into the line was sufficient to vaporize a part of the liquid flow at low flow rates. In order to overcome this problem, a bleed port was provided just prior to the nozzle. Thus, the total flow through the line could be maintained high enough to prevent vaporization. The bleed flow was vaporized by passing it through a long heat exchanger

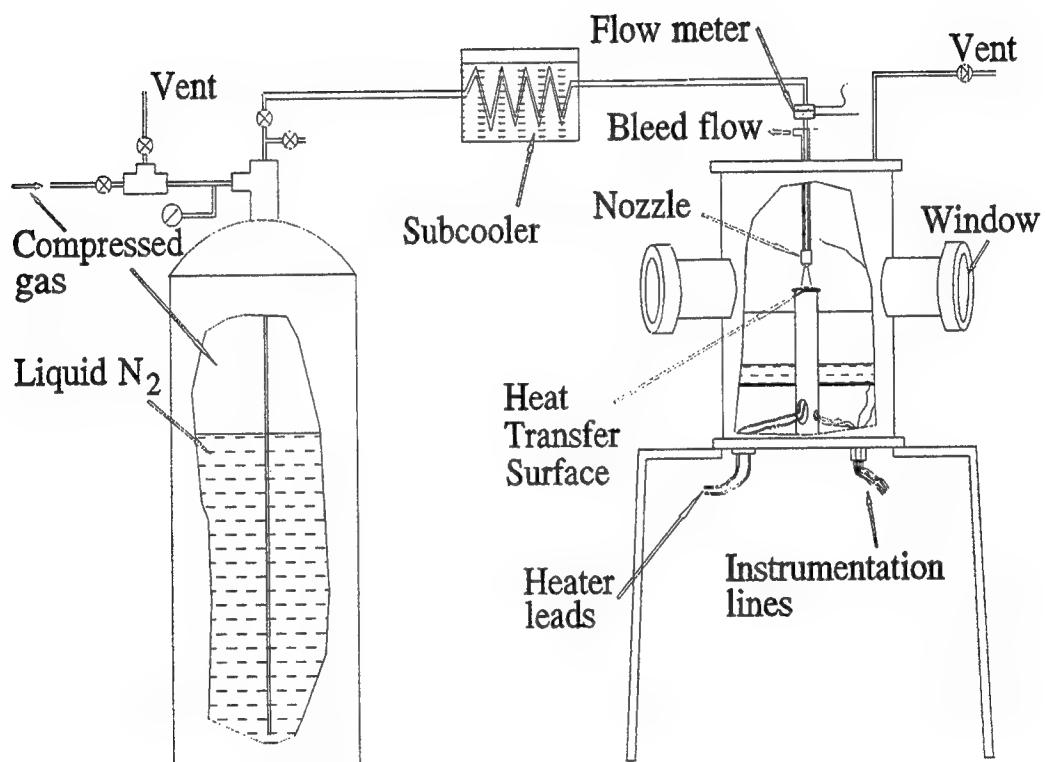


Figure 4.1 Spray Cooling Experimental Set-Up

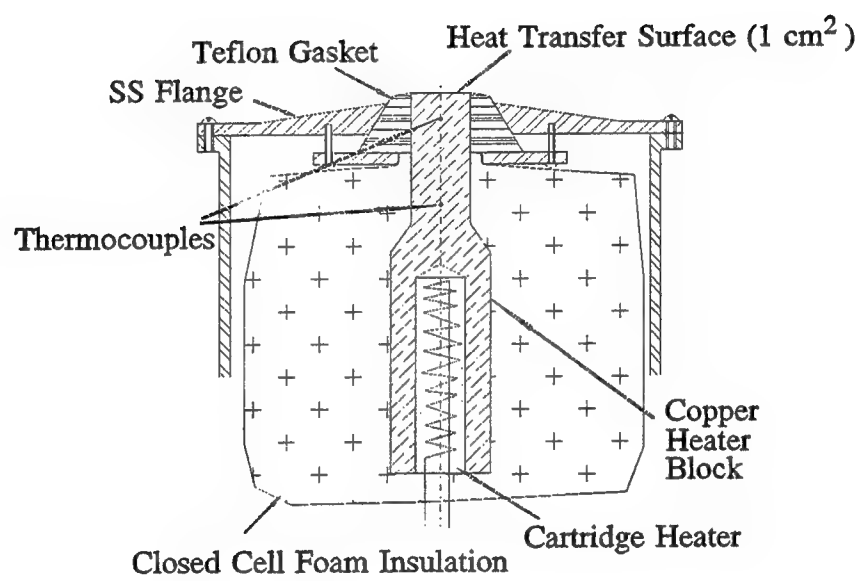


Figure 4.2 Heater Design

tube coil placed in a hot water bath. The bleed flow was continuously monitored by a mass flow meter measuring the flow rate of gaseous nitrogen exiting the heat exchanger.

The heater, shown in Figure 4.2, is made out of oxygen free copper; a cartridge heater inserted inside the copper block provides the heat. The power to the cartridge heater is supplied by a variac. The heat transfer surface is a 1-cm² circle on the top of the block. A cylindrical Teflon gasket was fitted onto the top part of the block. The fit between the Teflon gasket and the copper block was very tight and provided a very good seal against liquid leakage into the interface. The top surface of the block (the heat transfer surface) was made flush to the top surface of the teflon gasket as shown in the figure. Two thermocouples in the copper block below the heat transfer surface measure the temperature gradient below the surface. The optimum thermocouple distance from the surface was obtained by thermal design using ANSYS (Finite Element Analysis software by Swanson Analysis Systems, Inc.). The thermocouple distance was sufficient to enable extrapolation of average surface temperature even if a moderate lateral temperature gradient existed on the surface (a 5 K lateral gradient was used to obtain the design values). The heat flux and the average surface temperature is estimated from these thermocouple measurements. All surfaces of the heater block except the top are insulated using polyurethane foam (thermal conductivity: 0.035 W/m.K) to prevent heat loss. The heat loss from the block was estimated to be less than 2% with this insulation (based on calculations assuming that the outer surface of the insulation is at LN2 temperature). The heat input from the cartridge heater is determined by measuring the power input to the heater using a power transducer. This measurement was used to confirm the heat flux calculated from the temperature gradient and validate those calculations.

In addition to those in the copper block, thermocouples were also placed on the insulation surface, inside the chamber, on the nozzle body, in-stream near nozzle inlet, in the subcooling heat exchanger and on the chamber surface. The liquid flow rate to the nozzle is calculated by subtracting the bleed flow rate from the flow rate measured by the orifice-flow-meter shown in Figure 4.1. All of the thermocouples and the power transducer output were read by a Fluke Helios Plus data acquisition system connected to a PC.

4.2 Experimental Procedure

An experimental run involved spraying the LN2 at a certain pressure and 78 K through

the nozzle onto the heater surface. The roughness of the heater surface was measured before the heater was installed in the chamber, and also at the conclusion of the whole set of experiments. The roughness was measured by a surface profilometer (Surtronic 3P, Rank Taylor-Hobson Ltd.) and was around $R_a = 0.15 \mu\text{m}$ both before and after the experiments. The surface was cleaned with a very dilute solution of hydrochloric acid and then rinsed with deionized distilled water and propanol prior to each set of experiments. Before beginning the experiment, the chamber is flushed with nitrogen to expel any air or water vapor. The subcooling heat exchanger shell is filled with LN2 and the fluid is allowed to flow from the dewar to the nozzle. The bleed port is kept fully open till the line cools down to LN2 temperature. This is evidenced by the temperature of the nozzle reaching 78 K. The pressure of the dewar is then set at the desired value by venting the dewar or pressurizing it from a N2 gas cylinder. The bleed valve is adjusted till the bleed flow is as low as possible while still sufficient to maintain the nozzle temperature at 78 K. The bleed flow rate never exceeded $4.0 \times 10^4 \text{ kg/hr.m}^2$. The nozzle height and alignment is adjusted to ensure that the spray covers the whole heat transfer surface and all the spray impinges the surface.

The power to the heater cartridge is then increased gradually till dry-out of the surface occurs. After each step increase in power, sufficient time is allowed for all the temperatures to reach steady state. The power to the heater is cut off immediately following the dry-out. Dry-out is evidenced by the rapid increase in temperature readings of the two thermocouples inside the copper block. Upon dry-out, the temperature of the surface usually reaches about 200 K because of the thermal inertia of the heater block. The data recording is continued till the surface temperature falls back to about 80 K under the same spray conditions. Although these cool-down readings are not at steady state, the correct heat flux and surface temperature can be estimated by correcting for the temperature transients. The cool-down readings provide the heat transfer characteristics for LN2 spray cooling in the Leidenfrost point region.

In general, a set of runs were taken consecutively till the LN2 in the dewar ran out, or, the nozzle had to be changed. The set of results presented here involved four nozzles: TG0.3, TG0.5, TG0.7 and FLNo.13. The TG series nozzles are full cone pressure atomizing nozzles commercially available from Spraying Systems Co., Wheaton, IL. These nozzles have a flow swirler before the orifice which creates turbulent flow for effective atomization. The FLNo.13 is a flat disc shaped nozzle with radial grooves leading to the orifice (for creating turbulence).

The orifice diameters for these nozzles are presented in Table 4.1.

Table 4.1 Nozzle Size

Nozzle	Orifice Dia. mm
TG0.7	0.76
TG0.5	0.61
TG0.3	0.51
FLNo.13	0.38

The experiments were carried out for five to six different pressures for each nozzle (207, 276, 414, 552, 690 and 828 kPa). The nozzle inlet pressure was continuously monitored by a Bourdon gauge connected to the low pressure side of the orifice-meter. The spray cone for the FLNo.13 nozzle (about 30°) was much narrower than that for the TG series nozzles (about 60°). The nozzle height above the surface was varied to keep the surface covered with spray, all the experiments with TG series nozzles had approximately the same nozzle height: 1 cm; the height for the FLNo.13 nozzle was 1.6 cm. The nozzle height was adjusted such that the spray cone hit the whole surface and did not extend beyond it. All the nozzles used in this study had no nonuniformities in the angular direction (i.e. the spray cones always had a circular cross-section). The spray parameters: droplet size distribution and velocity distribution were measured by a phase Doppler particle analyzer (PDPA). These parameters could be measured using the PDPA system through the windows provided on the experimental chamber. The spray parameters of importance are the droplet size and velocity distribution at the heat transfer surface. These parameters were measured at appropriate distance from the nozzle exit (1 cm for TG nozzles and 1.6 cm for FLNo.13 nozzle). Thus the droplet velocity and size distributions at various radial positions in the plane perpendicular to the nozzle axis were measured for each nozzle at the same flow conditions used in the heat transfer experiments.

4.3 Uncertainty Analysis

The heat flux is measured by using the temperature gradient readings provided by the two thermocouples in the copper block (using Fouriers's law: $q'' = k\Delta T/l$). Hence, the uncertainty in heat flux measurement is related to the uncertainty in the measurement of temperature

difference between the two thermocouples in the copper block. The manufacturer specified uncertainty in the temperature measured by E-type thermocouples is 1.7 K. However, at a heat flux of 0 W/m^2 (at 78 K), the two thermocouples always read within $\pm 0.25 \text{ K}$. Thus, this is a better measure of the error in ΔT . The relative uncertainty in thermal conductivity of copper ($\Delta k/k$) is 0.02. The two thermocouples are located in holes which have a diameter of 0.5mm each and are 16.5mm apart (center to center distance). The relative uncertainty in distance between the thermocouples ($\Delta l/l$) is therefore 0.06. Hence, the maximum relative uncertainty in heat flux measurement comes to $0.08 + 0.25/\Delta T$. This uncertainty decreases with increase in ΔT . Near critical heat flux the ΔT is usually on the order of 50 K. Thus, the uncertainty in CHF is close to $\pm 8\%$.

The surface temperature is calculated by extrapolation from the two thermocouple readings. The maximum uncertainty in surface temperature was found by calculations to be 3.0 K at a heat flux of 1500 kW/m^2 . The nozzle pressure is measured by a gauge having a least count of 13.8 kPa (2 psig). Since, the mass flow rate is estimated by using an orifice-meter, the uncertainty is composed of the error in pressure drop measurement and the error in discharge coefficient (C_d). The differential pressure transducer has an uncertainty of 2%, and the uncertainty in C_d is about 3%. Thus the uncertainty in mass flow rate is $3 + 0.5(2) = 4\%$.

4.4 Results and Discussion

Since most of the LN2 spray cooling heat transfer data used in this study was reported in a previous report [22], the results of spray parameters measurements are presented first. The measurements were carried out by an Aerometrics PDPA system having the ability to measure the droplet size distribution and the velocity along a single flow direction. The velocity distribution data obtained during the experiments were very repeatable and easy to obtain. The same was not true for the droplet size distribution. Since the sprays produced during these experiments were very dense and consisted of very fine droplets, the PDPA system had a great difficulty in providing consistent data. Also, the very nature of optical measurements biases the instrument in favor of the larger droplets.

The dense nature of the spray prevented the droplet diameter data collection for high pressure cases for all the nozzles. The reliability of the data is related to the validations/samples ratio. The PDPA system uses three in-line detectors to collect the phase shift data which is used

Table 4.2 Spray Parameters.

Nozzle	Pressure kPa	G kg/m ² s	d (SMD) (Eqn. 1) μm	Velocity m/s
FL#13	276	16.9	21	16.0
	414	20.3	18	18.5
	552	23.3	16	20.3
	690	25.6	15	22.6
	828	27.8	14	24.2
TG0.3	276	20.6	22	14.0
	414	24.9	19	15.1
	552	28.4	17	18.3
	690	31.3	15	19.7
	828	34.1	14	21.0
TG0.5	207	37.3	29	15.4
	276	42.8	26	17.9
	414	51.4	22	21.8
	552	58.9	20	25.4
	690	65.0	18	28.5
	828	70.6	17	30.7
TG0.7	276	55.4	28	19.0
	414	66.7	24	21.6
	552	75.8	21	23.1
	690	82.8	19	24.8
	828	88.9	18	27.1

to calculate the droplet size. Thus, it takes two readings of the phase shift of the doppler signal, between the first and second, and, the second and third detector. If the readings do not match, more than one droplet was probably present in the probe volume and that sample is, therefore, rejected. Thus, the system provides a validations/samples ratio which is a measure of the reliability of the spray distribution characteristics measured. The validations/samples ratio for droplet diameter measurements was too low to be reliable in most cases. Even for the low pressure sprays this ratio was as low as 0.6, i.e., almost half the data samples were rejected.

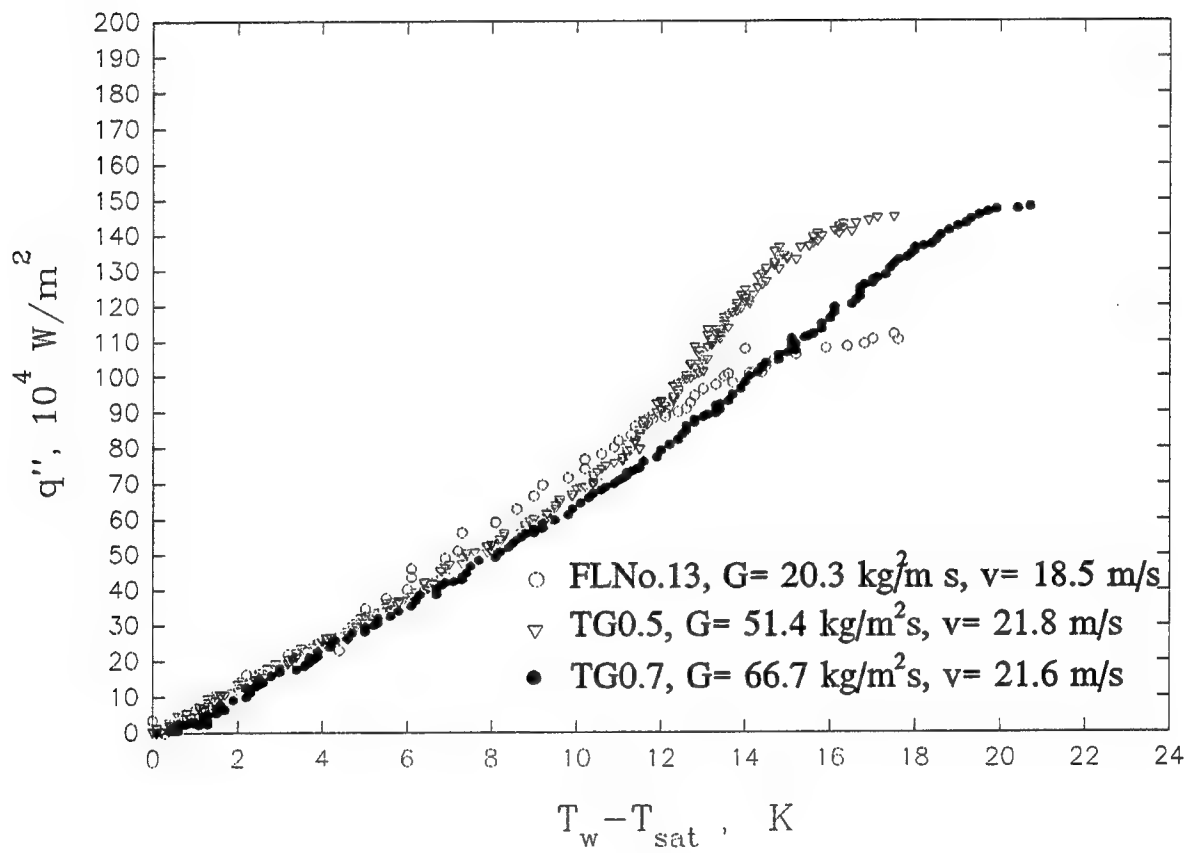


Figure 4.3 Spray Cooling Characteristics of Different Nozzles.

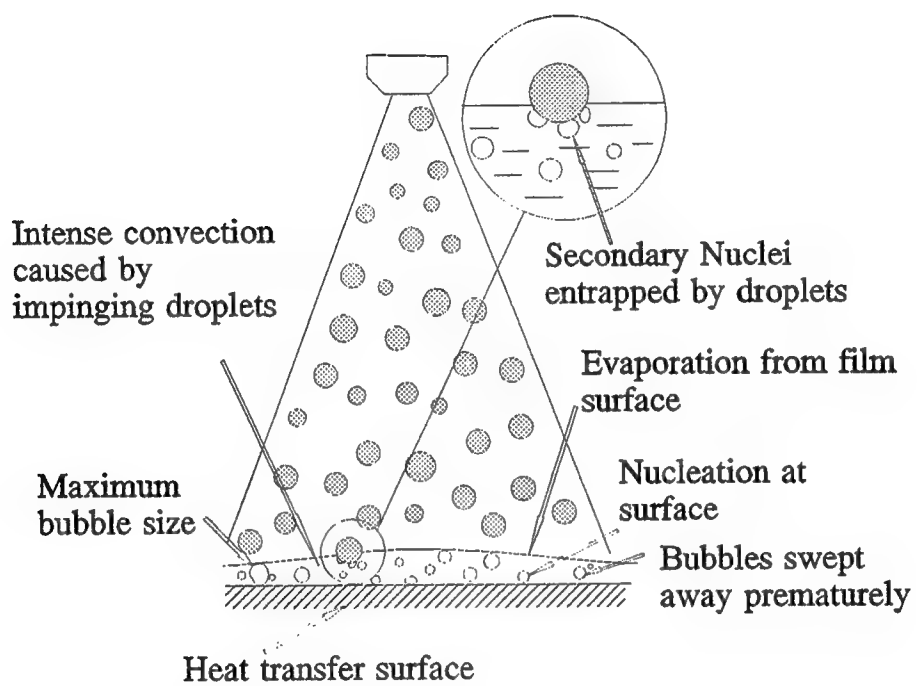


Figure 4.4 Spray Cooling Physics.

Since reliable data on the Sauter mean diameter (SMD) could not be obtained for the majority of cases, a correlation for SMD had to be used. Lefebvre [21] suggested a general correlation for SMD based on extensive data and literature survey. This correlation, shown here

$$d = 2.25 \sigma^{0.25} \mu_f^{0.25} \dot{m}_f^{0.25} \Delta P_f^{-0.5} \rho_g^{-0.25} \quad (4.1)$$

as Equation 4.1, showed reasonable agreement to the experimental data that was obtained (the symbol d used henceforth represents the SMD of the spray). Table 4.2 shows the SMD values predicted by the correlation. These values of SMD were used for data reduction purposes.

The velocity distribution from the measurements was reasonably repeatable and could be considered reliable. The velocity distribution for any location was always Gaussian with a standard deviation of 2-4 m/s. The spray velocity as a function of the radial position in the spray was also obtained. In all cases, the velocity distribution was fairly constant for most of the spray, however, the velocity falls off very sharply close to the spray edge. This is probably due to the fact that the outermost droplets suffer significantly more drag compared to those inside the spray cone. The average velocity variation with the radial position was similar for all the nozzles used in this study. Hence, the mean velocity at the center can be considered as the representative velocity for a spray condition. Table 4.2 shows the average velocities at the center for the test cases. These values were used in conjunction with the SMD values obtained from Equation 4.1 to obtain the correlations presented later in this paper.

The detailed results from the heat transfer experiments have been reported in the previous report [22]. For the purpose of discussion, a set of results are provided here. Figure 4.3 shows the heat transfer characteristics of spray cooling with three different nozzles at the same inlet pressure (414 kPa) and similar surface roughnesses ($R_a = 0.05 \mu\text{m}$). As shown in the figure, the CHF seems to increase with the spray velocity. The trend in heat transfer characteristics is however not very clear.

A brief discussion of spray cooling theory will provide a better insight into the results presented here. Figure 4.4 shows the probable mechanisms involved in spray cooling heat transfer. Convection heat transfer, evaporation from the film surface, nucleate boiling at the heater surface and secondary nucleation are all thought to be involved in spray cooling. The intense convection caused by impinging droplets enhances the heat transfer between the heater surface and the free surface of liquid film, the heat transferred to the film surface goes towards

evaporation of the fluid. Nucleate boiling at the heater surface with premature bubble removal also helps in increasing the heat transfer coefficient greatly. Since a spray with high speed droplets is subjected on the liquid film surface, the bubbles growing in the liquid film are unlikely to survive once their size approaches the liquid film thickness. Thus, the bubbles can breakup at a very small size, even before the microlayer [23,24] is completely evaporated. This bypasses the much longer and less efficient growth period in pool boiling where the bubble has to grow slowly after microlayer evaporation in order to attain enough volume for the buoyancy forces to overcome the surface tension forces holding the bubble to the surface. The overall effect of this premature bubble breakup is to increase the net time the microlayer evaporation exists on a surface and thereby increase the heat transfer coefficient. Finally, secondary nucleation, which results from the entrapment of vapor bubbles by impinging liquid droplets, also play a very important role in spray cooling [25, 26]. The term secondary nucleation was coined to describe the nuclei from the vapor entrained by the reentering droplets created by bubbles bursting out of the liquid film. Due to the lack of a better term and due to the fact that the phenomenon is similar whether the droplets originate from the liquid film, or from an external source, spray in this case, we refer to nucleation due to vapor entrained by the spray as secondary nucleation. Also, due to the very high number density of spray droplets impinging on the liquid film the dominant source of this secondary nucleation is the spray itself. The heat transfer due to secondary nucleation would be less efficient as compared to microlayer evaporation since the thickness of liquid between a secondary nucleus and the heat transfer surface is larger than the microlayer thickness. Although it is conceivable that a bubble due to a secondary nucleus can get close enough to the heat transfer surface to permit microlayer evaporation, the time for this type of microlayer evaporation is unlikely to approach that experienced by a bubble originating from a surface cavity. Hence, it is safe to assume that bubbles originating from surface cavities remove heat more efficiently as compared to bubbles originating away from the surface.

The relative importance of each of these heat transfer mechanisms is unknown to date, but in spite of the lack of that information, the hypothesis provides a useful tool for evaluating the experimental results. Also, the experimental data will help in resolving the various issues involved in the hypothesis. Another point which has to be stated is that the hysteresis phenomenon, which is quite common in boiling from surfaces in highly wetting liquids like

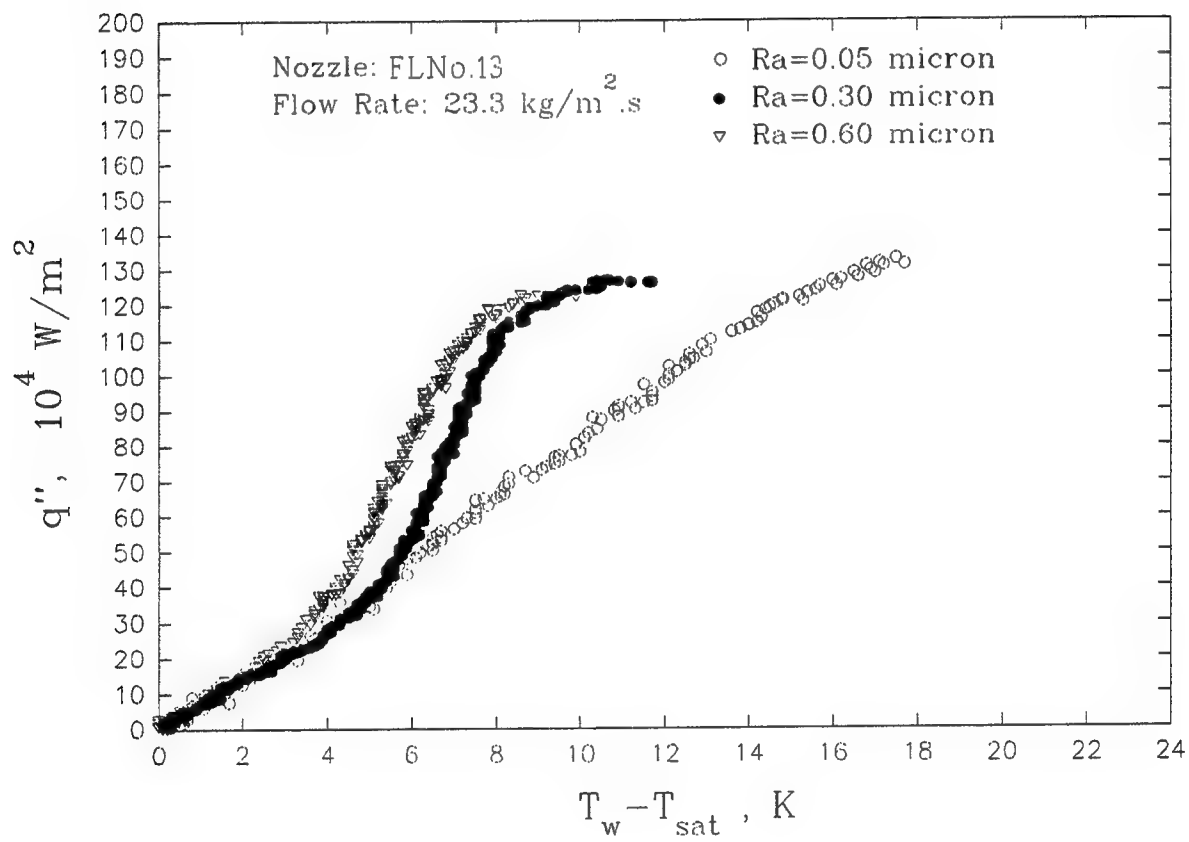


Figure 4.5 Effect of Surface Roughness.

chlorofluorocarbons and cryogens, is not expected to occur in spray cooling. This is due to the fact that the presence of secondary nucleation facilitates phase change at very low superheat and thus prevents the temperature overshoot which occurs due to deactivation of nucleation sites on the surface.

As seen from Figure 4.3, the heat transfer curves are made up of three distinct regions. The first is the low superheat region. Here, the heat transfer is probably dominated by forced convection with evaporation from the film surface and secondary nucleation. Nucleate boiling *from the surface* is absent in the first region because surface nucleation requires a higher superheat under forced convection situations and would be noticeable by a distinct change in slope [27]. On the other hand, boiling due to secondary nucleation can exist from a very low superheat and would be undeterminable from the heat transfer curve in this case. As the superheat is increased, the slope of one of the curves shows a small jump at about 10 K superheat. This is probably due to the beginning of nucleate boiling from cavities on the heater surface. As mentioned earlier, nucleation from the surface cavities allows microlayer evaporation and hence higher heat transfer coefficient as compared to nuclei originating in the liquid film. Hence, this shift in slope could be attributed to the boiling from nucleation sites on the surface. Once the nucleate boiling from the heater surface has begun, the same curve shows a definite shift upwards, this second region has a significant contribution by surface nucleation. However, since this did not occur for all the cases, it was felt that the change in slope for some of the cases could have been caused by undetectable changes in the heat transfer surface (presence of oxide layer). The final region is a flattening of the curve leading to the CHF, this is similar to the behavior seen in flow boiling situations. In order to investigate the effects of surface conditions, which seemed to play a role in the previous experiments, some experiments were conducted as part of the present study.

The roughness of the heat transfer surface was varied to investigate the effect of surface conditions. Three different surface roughnesses were tested. The average roughness (R_a) values of the test surfaces were: 0.05, 0.3, and 0.6 μm (measured with a Rank-Taylor 3P profilometer). Figure 4.5 shows the difference in heat transfer characteristics for the three surfaces. It is clear from the figure that the surface roughness makes a significant difference in the heat transfer phenomena. Clearly the smoothest surface shows no abrupt change in slope whereas the two rougher surfaces show a significant shift in slope as superheat increases. The temperature at

which this shift in slope occurs, decreases with increase in surface roughness. This is a clear indication of change in surface nucleation characteristics. As reported by numerous researchers, the temperature for onset of nucleate boiling decreases as the surface roughness increases. In the present case, this clearly points to the fact that the rougher surfaces show surface nucleation while the smoothest surface does not. Since surface nucleation is much more efficient as compared to secondary nucleation and surface evaporation, the presence of surface nucleation causes a significant increase in the heat transfer rate for the rough surfaces. The smoothest surface continues to have the same heat transfer coefficient with increase in superheat. This indicates an absence of surface nucleation.

These results prove the speculation that the shift in slope for some cases was due to small differences in surface conditions. This effect is especially significant for a highly wetting liquid like LN₂. The surface nucleation cavities for the smooth surfaces are easily deactivated by flooding, hence surface nucleation is suppressed on smooth surfaces.

The CHF for the different roughness surfaces are within a spread of 5%; since the CHF is very sensitive to experimental conditions, this deviation is not so significant. Some other experiments conducted at other flow rates showed a slight increase in CHF for rougher surfaces. Hence, it was felt that the differences in CHF were due to experimental uncertainties and not due to the surface roughness. This leads us to the conclusion that CHF mechanism is the same irrespective of the surface condition.

The contribution of surface nucleation is negligible for the smoothest surface while it is significant for the rougher surfaces. Since only 30 % of the liquid evaporates at the maximum heat flux for the case shown in Figure 4.5, the CHF is not caused by lack of liquid. There are two conditions under which the CHF mechanism can be the same regardless of surface condition. First, if the vapor generation at the surface is significant, the vapor flow can entrain the incoming droplets and prevent liquid replenishment on the surface. Second, if secondary nucleation is significant, the total bubble generation in the liquid film on the smoothest surface could approach the bubble generation due to surface nucleation on the rough surfaces. Thus a vapor layer in the liquid film can choke off the liquid supply to the surface. The first condition is not very likely; if we assume that the vapor generated from the surface flows only upwards, the vapor velocity at CHF would be about 1.3 m/s. This is an order of magnitude lower than the average droplet velocities, hence, it is unlikely that the droplets can be entrained by the

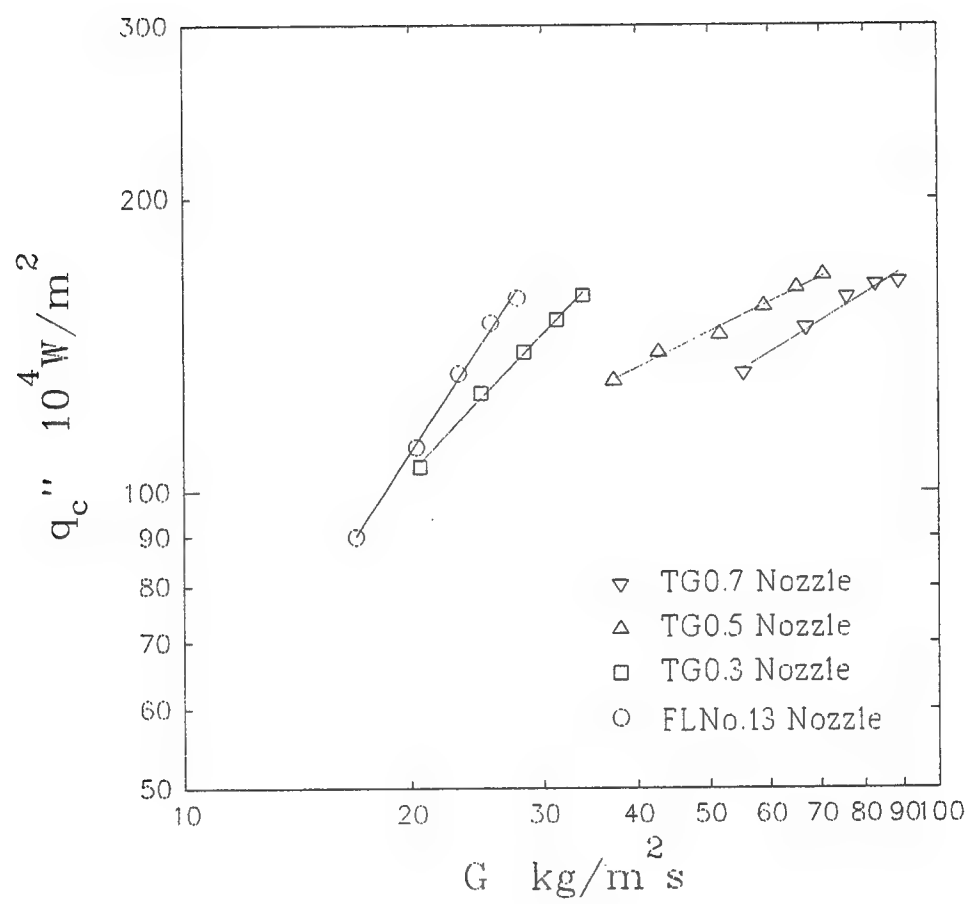


Figure 4.6 CHF versus Mass Flow Rate for Different Nozzles.

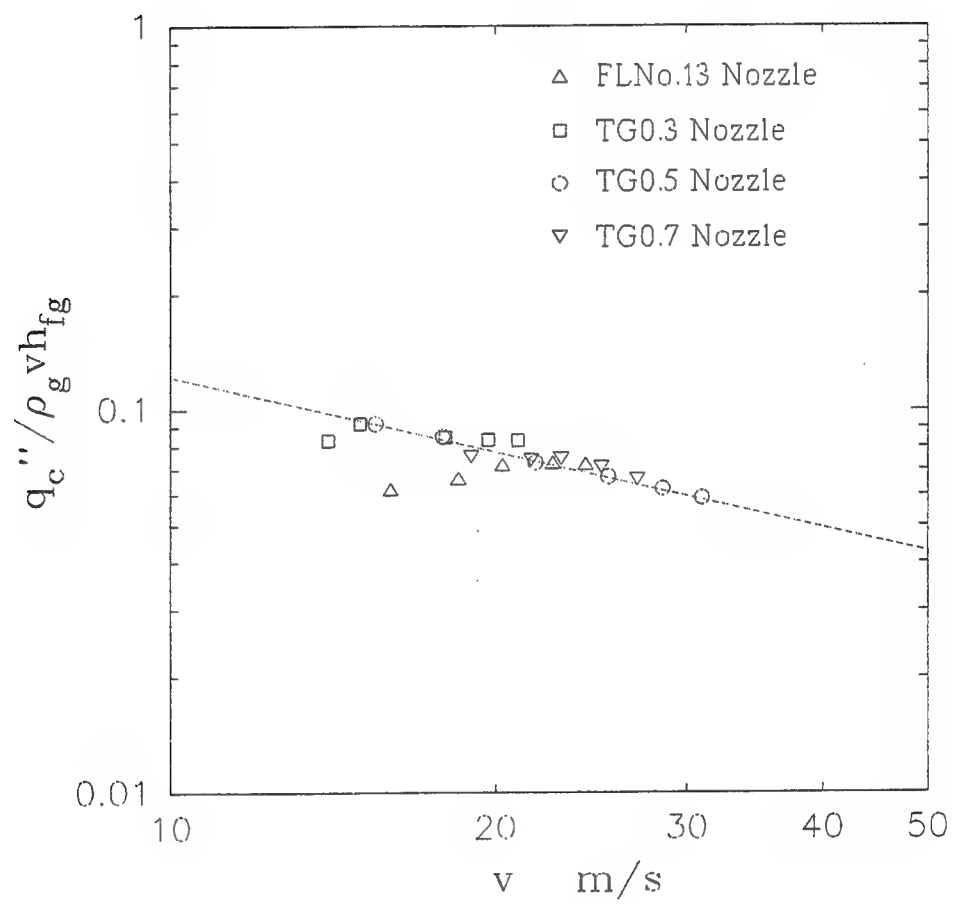


Figure 4.7 CHF Dependence on Velocity.

vapor flow. Hence, it is very likely that the bubble generation in the liquid film gives rise to CHF conditions. The exact CHF mechanism is not clear since the visualization of the flow in the liquid film formed by the flow is all but impossible.

4.5 Data Reduction and Correlation Development

One of the major difficulties in analyzing spray cooling lies in isolating the various spray parameters. The droplet velocity, diameter, and the volume flow rate are directly related to the nozzle pressure for a particular nozzle. This was the reason for selecting different nozzles for the study. The range of parameters for this study were: $SMD = 14\text{--}29\ \mu\text{m}$, the velocity = $14\text{--}31\ \text{m/s}$, and the mass flow rate = $16.9\text{--}88.9\ \text{kg/m}^2\text{s}$.

4.5.1 Critical Heat Flux

The maximum effectiveness of the spray cooling ($q''/h_{fg}G$) for this study was never above 35%, hence, the CHF was not caused by a lack of liquid (as is the case for low flow rate mist cooling situations). The CHF is caused by the inability of the liquid to reach the surface at a sufficient rate. This could be due to the formation of vapor blankets in the liquid film. This noncontinuous vapor blanket chokes off the supply of the liquid to the surface gradually as the temperature is increased. The cause of the formation of the vapor blanket can be the bubbles formed at the heat transfer surface, or, the bubbles formed due to secondary nucleation. Figure 4.6 shows the critical heat flux vs. mass flow rate data from the previous report [22]. It is clear from the figure that the mass flow rate is not a good representative of the CHF. Although the CHF increases with mass flow rate for each nozzle, that increase could just be a function of increased spray velocity. Hence, a comparison of nondimensional vapor velocity with average spray droplet velocity is shown in Figure 4.7. In this case, the trend is very clear. A diminishing return for increase in velocity is seen from this figure.

In an earlier spray cooling study done by Monde [28], it was reported that for high liquid flow rate spray cooling, the CHF follows the same dependence on velocity as in jet impingement process. In a more recent study, Monde presented a generalized correlation for jet impingement CHF [29]. The CHF was given by Equation 4.2 shown here. This correlation was based on a hydrodynamic model developed by Haramura and Katto [30] and Katto [31] for forced convection boiling. The strong dependence on D/d_j (here, d_j is the jet diameter) for jet

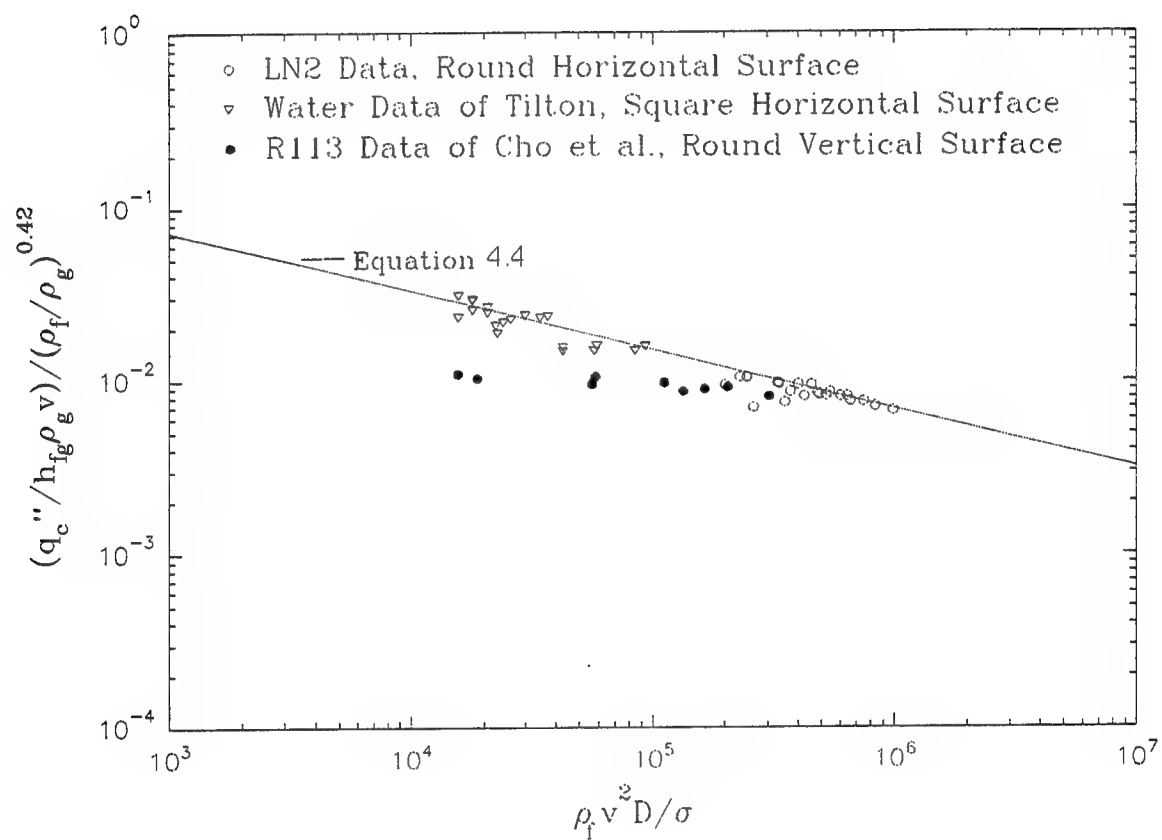


Figure 4.8 CHF Correlation Comparison.

impingement is obvious, because, as this ratio increases, the earlier the CHF occurs. However, the same cannot be said about spray cooling. Here, a correlation essentially similar to Equation 4.2 is attempted (Equation 4.3). Since the effect of d/D ratio on spray cooling is not clear, it was included as part of the attempted correlation.

The values of C_1 , a , b and c were found from a best fit of the LN2 spray cooling data and water spray cooling data of Tilton [15]. The water data were obtained by using slightly subcooled water spray on a horizontal square heater (1 cm^2). Hence, hydraulic diameter of the surface was used as D . Thus we get the final form of the spray cooling CHF correlation as Equation 4.4. As seen from the equation, the d/D ratio was found to have no significant influence on the CHF.

$$\frac{q_c''}{\rho_g h_{fg} v} = 0.22 \left(\frac{2\sigma}{\rho_f v^2 (D-d_j)} \right)^{0.343} \left(1 + \frac{D}{d_j} \right)^{-0.364} \left(\frac{\rho_f}{\rho_g} \right)^{0.645} \quad (4.2)$$

$$\frac{q_c''}{\rho_g h_{fg} v} = C_1 \left(\frac{\sigma}{\rho_f v^2 D} \right)^a \left(\frac{D}{d} \right)^b \left(\frac{\rho_f}{\rho_g} \right)^c \quad (4.3)$$

$$\frac{q_c''}{\rho_g h_{fg} v} = 0.76 \left(\frac{\sigma}{\rho_f v^2 D} \right)^{0.34} \left(\frac{\rho_f}{\rho_g} \right)^{0.42} \quad (4.4)$$

Figure 4.8 shows the comparison of the Equation 4.4 to the data for LN2, water, and R113 from previous studies. The data from the R113 study was not used in developing the correlation since that study was performed on a vertically oriented surface [32].

The agreement to the water and LN2 data is quite good for an instability based phenomena like CHF. It should be mentioned that the exponents of the Weber number is similar to the correlation for jet impingement. However, the density ratio exponent is a little lower. The major difference is the lack of dependence on D/d ratio for spray cooling.

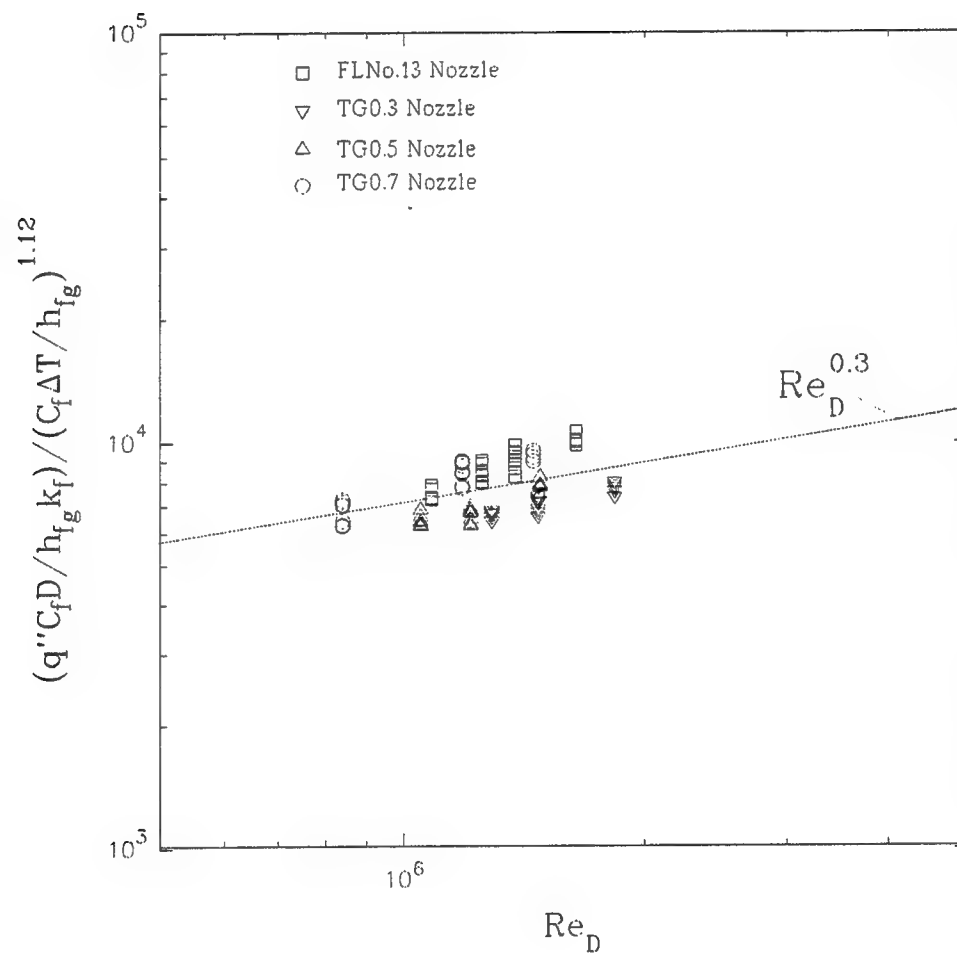


Figure 4.9 Heat Flux Dependence on Reynolds Number.

The lack of dependence on the D/d ratio for spray cooling gives it enormous advantage over jet impingement cooling. If Equation 4.2 and 4.4 are compared, it becomes obvious that the jet diameter, d_j , has to be close to $D/2$ to provide the same CHF as spray cooling (for LN2, at similar velocities). Since a high velocity spray can be obtained even with very small nozzle orifices, the mass flow rate required in spray cooling is not very high. However, in the case of jet impingement, the mass flow rate will have to be much higher due to high d_j (except for cases with extremely small D where d_j will be similar to the spray nozzle orifice diameter).

4.5.2 Heat Flux

Due to the lack of understanding of the fundamental processes involved in spray cooling, it is difficult to carry out the data reduction for heat flux. The difficulty lies in selecting the proper nondimensional variables to describe the spray process. Previous researchers have mostly used the droplet Weber number to correlate the heat transfer characteristics. The heat transfer rate due to the impact of single droplets has been shown to be a strong function of the droplet Weber number. However, the droplet Weber number alone cannot describe the spray cooling phenomena due to the presence of multiple droplets.

To begin, the nondimensional heat flux parameter is defined as $q''C_f D/h_{fg}k_f$. This is essentially the Nusselt number multiplied by nondimensional temperature difference represented by $C_f \Delta T/h_{fg}$. As explained earlier, the heat transfer rate dependence on the temperature difference is a very strong function of the surface roughness. The correlation of heat transfer rate with surface roughness is beyond the scope of this study. Hence, the heat transfer correlation for the smoothest surface only is attempted here. This is adequate because most electronic surfaces can be classified as smooth ($R_a < 0.1 \mu\text{m}$). Since a departure from the heat transfer curve for the smooth case was observed for some cases of the data set, the whole data set cannot be used in the correlation. Thus, only the surface roughness independent section of the curves were used in the correlation for heat transfer rate, this involved superheats lower than 8 K for all cases.

The first step was to correlate the temperature dependence of the heat transfer rate. The nondimensional parameter, $C_f \Delta T/h_{fg}$, was used to correlate the temperature dependence of the heat flux, the best fit exponent was 1.12. Since the spray velocity was found to be the representative velocity of the liquid film for the CHF correlation, it was apparent that the heat

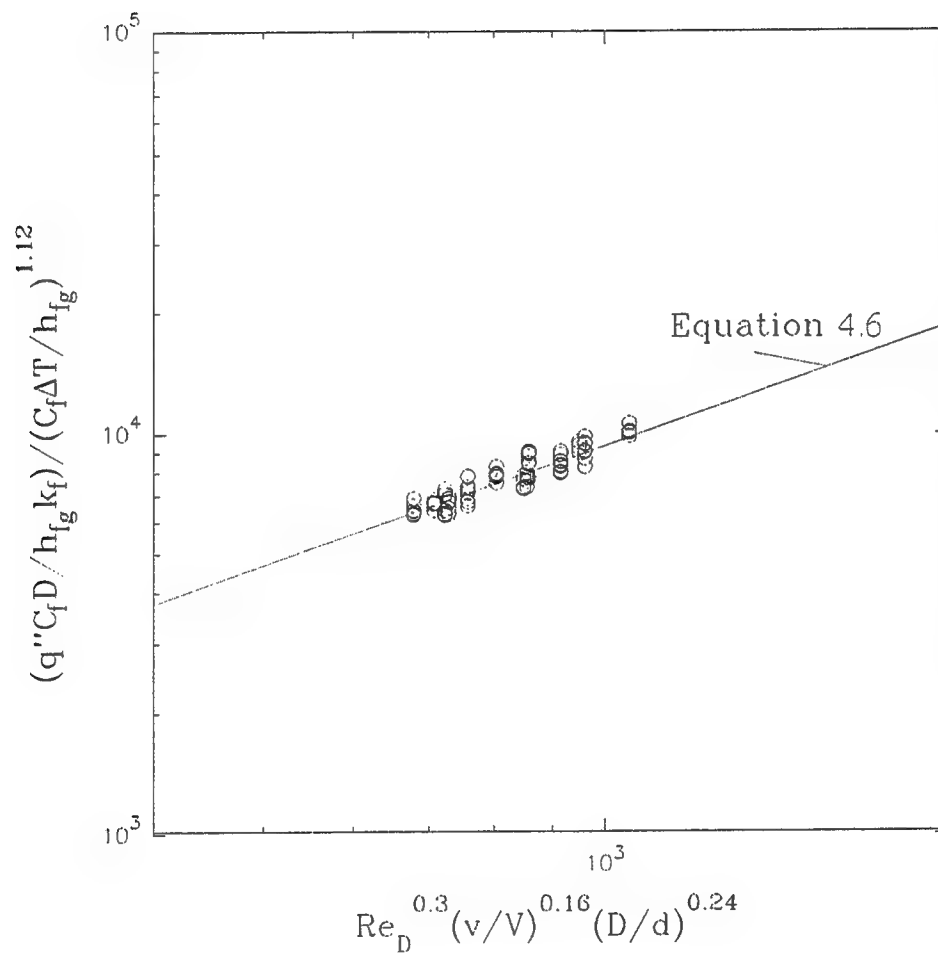


Figure 4.10 Spray Cooling Heat Flux Correlation.

flux would be a strong function of the liquid film Reynolds number based on the spray velocity too. Thus the temperature independent ratio, $(q'' C_f D / h_{fg} k_f) / (C_f \Delta T / h_{fg})^{1.12}$ can be plotted against the film Reynolds number (defined as $\rho_f v D / \mu_f$) as shown in Figure 4.9. As seen from the figure, the heat flux generally increases with the increase in Reynolds number. It is also clear that the Reynolds number is not the only parameter which has an effect on heat flux.

Another parameter which should have an immense effect on spray cooling effectiveness is the liquid film thickness. A thinner liquid film allows higher evaporation from the liquid surface and also permits the secondary nuclei to get closer to the heater surface. However, the liquid film thickness cannot be easily estimated. Hence, we define nondimensional velocity ratio, V/v , and droplet diameter ratio, d/D . The velocity ratio is one of the factors which controls the liquid film thickness. As the spray droplet velocity, v , increases for the same overall flow rate per unit area (V), the liquid film should be thinner due to the higher momentum of the incoming liquid. On the other hand, if the amount of incoming liquid, V , is increased keeping the droplet velocity the same, we should expect a thicker liquid film. The droplet diameter to surface diameter ratio, d/D , also influences film thickness. As the spray droplet size decreases, one would expect a thinner liquid film.

Using the nondimensional parameters defined above, the correlation for the spray cooling heat flux can thus be written as Equation 4.5. The exponents m , n , and p along with the coefficient C_2 were determined from a best fit of the data. Hence, we finally get the correlation for heat flux as Equation 4.6.

$$\frac{q'' C_f D}{h_{fg} k_f} = C_2 \text{Re}_D^m (V/v)^n (d/D)^p \left(\frac{C_f \Delta T}{h_{fg}} \right)^{1.12} \quad (4.5)$$

$$\frac{q'' C_f D}{h_{fg} k_f} = 9.4 \text{Re}_D^{0.3} \left(\frac{v}{V} \right)^{0.16} \left(\frac{D}{d} \right)^{0.24} \left(\frac{C_f \Delta T}{h_{fg}} \right)^{1.12} \quad (4.6)$$

The comparison of the correlation to the experimental data is shown on Figure 4.10. As seen from the figure, the agreement with the data is quite good. This suggests that the nondimensional numbers selected for the correlation are sufficient for the range of spray

conditions in this study. The Reynolds number has the maximum influence on the heat flux. The D/d ratio and v/V ratio also have significant influence, thus showing the importance of the liquid film thickness in spray cooling.

This correlation obviously does not contain all the necessary liquid properties necessary for applicability to other liquids. The Prandtl number and the density difference ratio, $(\rho_f - \rho_g)/\rho_g$, are the obvious candidates. A general empirical correlation could not be obtained for the lack of availability for data for liquids other than water in similar geometric configuration. Water is not a very good wetting liquid, hence, surface nucleation could exist from low superheats. Also, the water data was obtained at varying subcooling which were not reported. The data for other liquids were obtained for different geometries (R113 study of Ref. [32]) or the spray parameters were not available (Ref. [33]). Also, a better grasp of the factors influencing the liquid film thickness is needed. Hence, a general correlation for heat flux was not obtained. Also, given the large dependence of spray cooling heat transfer on the surface roughness, it should be noted that the correlation presented here applies only to spray cooling of smooth surfaces ($R_a < 0.1 \mu\text{m}$) with LN2.

5. POOL BOILING FROM A VERTICAL ARRAY IN LIQUID NITROGEN

Pool boiling in LN2 which has a reasonable maximum heat flux removal capacity ($1.6 \times 10^5 \text{ W/m}^2$ for horizontal surface under 1 atm., calculated using Zuber's model [12]) would be the easiest to apply in LNT electronic cooling. Though extensive studies have been conducted on pool boiling of LN2, they have mostly involved conventional pool boiling situations, i.e., single heat transfer surface in a pool of liquid [34,35]. However, the situation in most electronic equipment consists of a series of discrete heat sources which may interfere with the boiling phenomena on each other. Some researchers have speculated that the bubble layer generated by the presence of numerous heat sources on a vertical plate may create less favorable boiling conditions for the upper heaters [36]. However, no comprehensive study regarding the behavior of vertical heater array in LN2 pool boiling could be found.

The most likely configuration for electronic cooling in LN2 is probably a vertical array of chips having different heat dissipations on a circuit board immersed in LN2. In a case like this the chips on the bottom will give rise to a flow field which may influence the boiling heat transfer from all the chips above. Hence, the upper chips encounter more of a flow boiling condition instead of pool boiling. Although correlations exist for flow boiling from small size heaters [37], the flow field created on an upper chip due to boiling on a lower chip is difficult to estimate. A number of studies dealing with linear heater arrays under flow boiling conditions exist in literature [38-40]. However, the situation in pool boiling is totally different due to the fact that the flow velocity is dependent on the heat flux at various heaters, whereas, in these flow boiling studies, the flow velocity could be independently varied. Another point of difference is the distinction between a pool of liquid and a limited channel which exists in these flow boiling studies. The flow in channels is largely along the channel direction whereas in a pool the liquid is free to flow in any direction. A few studies dealing with vertical arrays in pool boiling were also found. You et. al [41] studied pool boiling heat transfer from a 3x3 array of 5mmx5mm heaters in gas-saturated FC-72. The distance between the heaters was 4mm in both directions. They found that boiling from a lower heater resulted in a decrease in the superheat overshoot (associated with boiling incipience in highly wetting liquids) at the upper heater. They did not observe any significant effect of the lower heater on critical heat flux of an upper heater. Another study, by Polentini et al. [42], involved nucleate boiling investigation from a 3x3 array

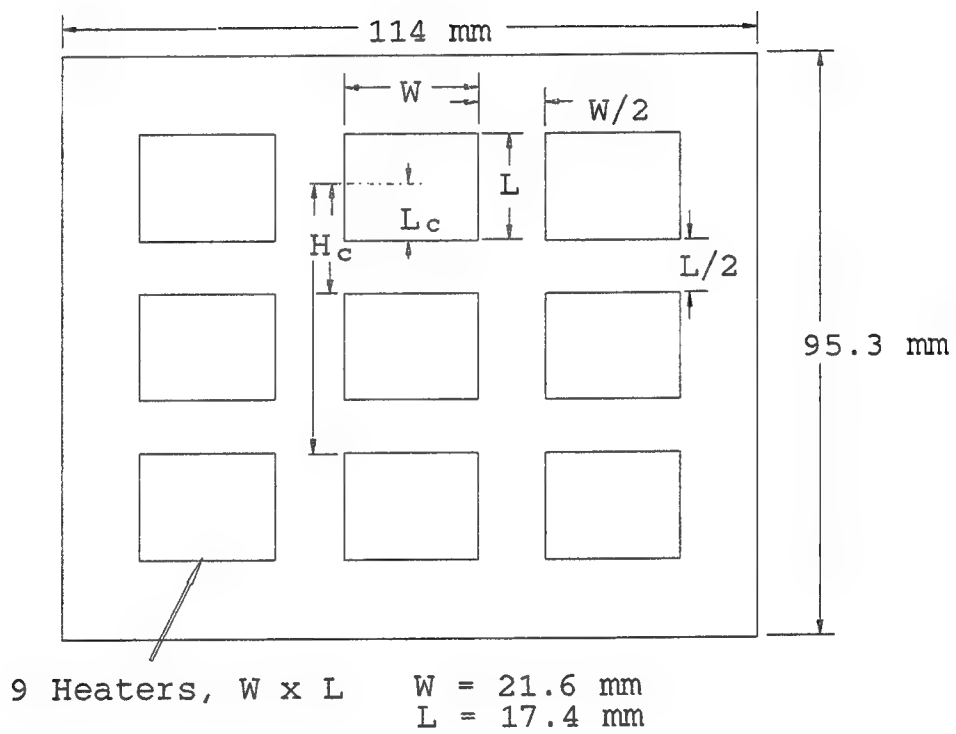


Figure 5.1 Heater Array Configuration.

(each heater 12.7mm x 12.7mm) in an enclosure containing FC-72 with two cold plates (maintained at 25 °C, 20 K below saturation temperature), one opposite the heater array (19mm away) and one on top. They reported a 15% increase in heat transfer coefficient from the middle heaters when the orientation was changed from horizontal to vertical. This was attributed to bubble pumped convection. Although they did not study the CHF conditions in detail, they reported that the CHF generally occurred at one of the heaters in the lowest row. Except for the study by You et al. [41], the other studies dealing with heater arrays only consider equal heat flux from each of the heaters. This situation is rare in electronics as different chips dissipate different amounts of heat. Hence, a need exists for studying the boiling characteristics from a bank of vertically oriented heat sources in LN2 with individual control of each heat source.

Thus, the purpose of this research effort was to study the boiling heat transfer from heat sources arranged in a vertical array in a pool of LN2. The experimental setup was designed to enable individual control of each heater in the array. The main points of interest were the influence of the flow field created by lower heaters on the heat transfer coefficient and critical heat flux (CHF) of the upper heaters. The following sections provide a description of the experiments conducted, the results and correlations for the areas of interest.

5.1 Experimental Set-up and Procedure

This study involved experiments for pool boiling heat transfer from a 3x3 vertical array of heaters. Figure 5.1 shows the heater array; the heaters are mounted flush to the surface of the plate. The bare chip size in electronics range from 5mmx5mm to a few hundred square mm. The critical heat flux (CHF) in pool boiling from liquid nitrogen is around $1.6 \times 10^5 \text{ W/m}^2$. This heat flux is modest, and therefore, many chips operating at LN2 temperature will require heat spreaders much like those in use for room temperature operation. Hence, the size of the heaters was chosen close to the commonly used chip sizes; each heater in the array was 21.6mm X 17.4mm (the rectangular shape allowed for two height-width combinations). The heaters have a sandwich construction, shown in Figure 5.2. An oxygen-free-copper heater block with an E-type thermocouple soldered at the center is soldered on to a ceramic substrate which has a thin resistor film deposited on its other face. Thus, the heat is provided by the film resistor and the temperature at the center of the heater is measured by the E-type thermocouple.

Nine of these heaters were mounted flush to a thin stainless-steel plate which was bolted

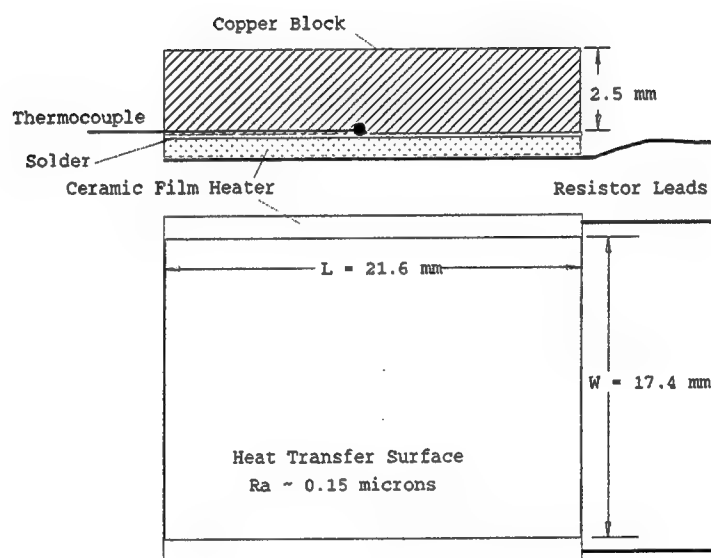


Figure 5.2 Heater Construction.

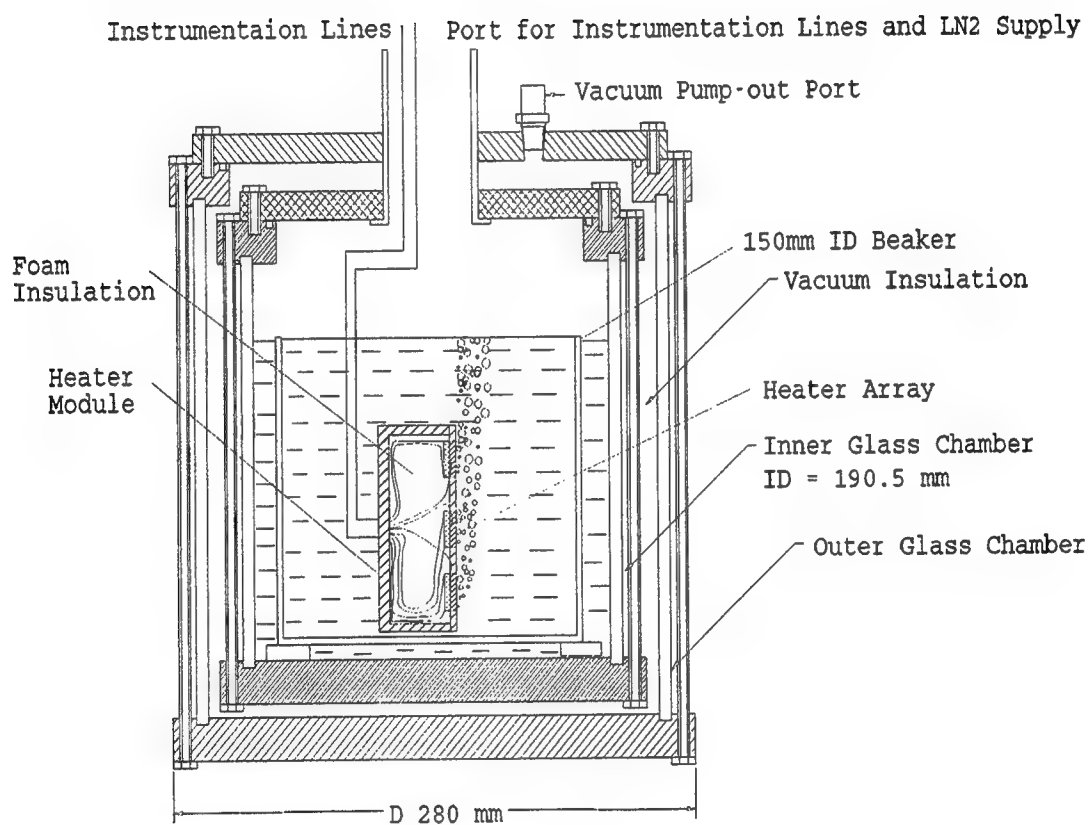


Figure 5.3 Schematic of the Experimental Set-Up.

on to the heater module casing shown in Figure 5.3. The heaters were insulated on the back with closed-cell foam insulation. A low conductivity epoxy provided the seal between the stainless-steel plate and the copper heater blocks. The heater and thermocouple leads pass through an opening in the back of the module, the feed-through hole is thoroughly sealed with closed cell foam to prevent liquid leakage into the module. The power input to each of the heaters can be individually controlled. All data, such as heater temperature and power dissipation, were collected by an IBM PC 386 through a programmed Hewlett Packard 3852A Data Acquisition/Control Unit equipped with a 5-1/2-digit voltmeter and a 20-channel relay multiplexer.

Figure 5.3 shows the details of the experimental set-up. Experiments were conducted in a seamless glass (borosilicate) cylinder with an inner diameter of 190.5 mm, and a height of 254 mm. It contained a pool of LN2 during the experiment. To prevent heat transfer from the environment, and allow for visualization of the boiling phenomena, this cylinder was placed inside another glass cylinder with inner diameter 240 mm. During preliminary experiments, it was seen that the cool-down time for the whole system was too long. Hence, a 150 mm-ID borosilicate beaker was placed inside the inner chamber, the whole chamber filled with LN2 and the heater module placed in the beaker. After this adjustment, the liquid pool inside the beaker became stagnant very quickly and this allowed for more efficient operation. The experiments were conducted at atmospheric pressure. The opening on top of the chamber (50mm in diameter) allowed for liquid refilling, heater and thermocouple wire feed-through, and vapor exhaust. The vapor exhaust flow was always enough to prevent any back-flow of room air (and moisture) into the chamber. Thus, any ice formation inside the chamber was avoided.

Before collecting each set of data, the heater surfaces were cleaned with dilute hydrochloric acid and deionized water to remove any oxides. The surface roughness of the heaters was measured by a surface profilometer. All the surfaces had average roughness, R_a , of around $0.15 \mu\text{m}$. Experiments were conducted at varying heat flux distributions. First, a particular heater was selected for study, this was usually one out of the uppermost heaters in the array. The inner glass chamber was filled with LN2. After the entire setup cooled down to LNT, one or both of the heaters below the selected heater were turned on and maintained at a constant heat flux. After the temperatures of the heaters reached steady state, the heat flux to the designated upper heater was increased. The heat flux was increased again when the heater

temperature restabilized. The process was repeated until the variable heater reached critical heat flux (CHF). This was indicated by a rapid increase in heater temperature. The power to the heater was shut off immediately on observing this temperature excursion. The boiling data for variable heaters with the other heat sources at 0 W/m^2 were also taken for comparison. After each trial, the pool of liquid nitrogen was replenished to the original level. The decrease in liquid level during the experiment was never more than 2-3 cm.

Since the heater module and the heaters were rectangular, experiments were conducted for both vertical orientations to investigate the influence of inter-heater distance and heater dimensions. The effects of different environmental conditions, such as varying bubble generation from surrounding heaters, were thus determined. In addition, the reproducibility of the data was determined by repeating some of the experiments. It was found that the heat transfer curve and the CHF were reproducible within the experimental uncertainty limits mentioned in the following section. The only data which was not reproducible was the temperature overshoot (typical of highly wetting liquids) prior to onset of nucleate boiling when only one heater was operating. In addition, the h and CHF data from different heaters under study was comparable when they were operated individually.

5.2 Uncertainty Analysis

The heat flux was estimated by measuring the power input to the heater and subtracting the estimated heat loss. The power input was measured by the product of dc voltage (error: $< \pm 0.01\%$) and the current (error: $< \pm 2\%$) across the heater/resistor. The maximum overall uncertainty in power measurement is therefore on the order of $\pm 2\%$. The heat loss from each heater was estimated by insulating the heat transfer surface and determining the $T-T_{\text{sat}}$ vs. power input curve (while the module is immersed in LN_2). This loss ranged from 300-400 $\text{W/m}^2\text{K}$ (calculated by dividing the power loss by the superheat and the heater area) for different heaters. The error in loss measurement does not cause a significant error in heat flux measurement because of the relatively small value of the loss. Thus, the accuracy of the heat flux estimate depends on the accuracy in power measurement and the accuracy of the heater area measurement ($\pm 0.7\%$). Taking all these into account, the uncertainty in heat flux was about $\pm 3\%$.

The E-type thermocouples used in the set-up have a manufacturer specified uncertainty of $\pm 1.7\text{K}$ at LN_2 temperature. However, since all the thermocouples were made with the same

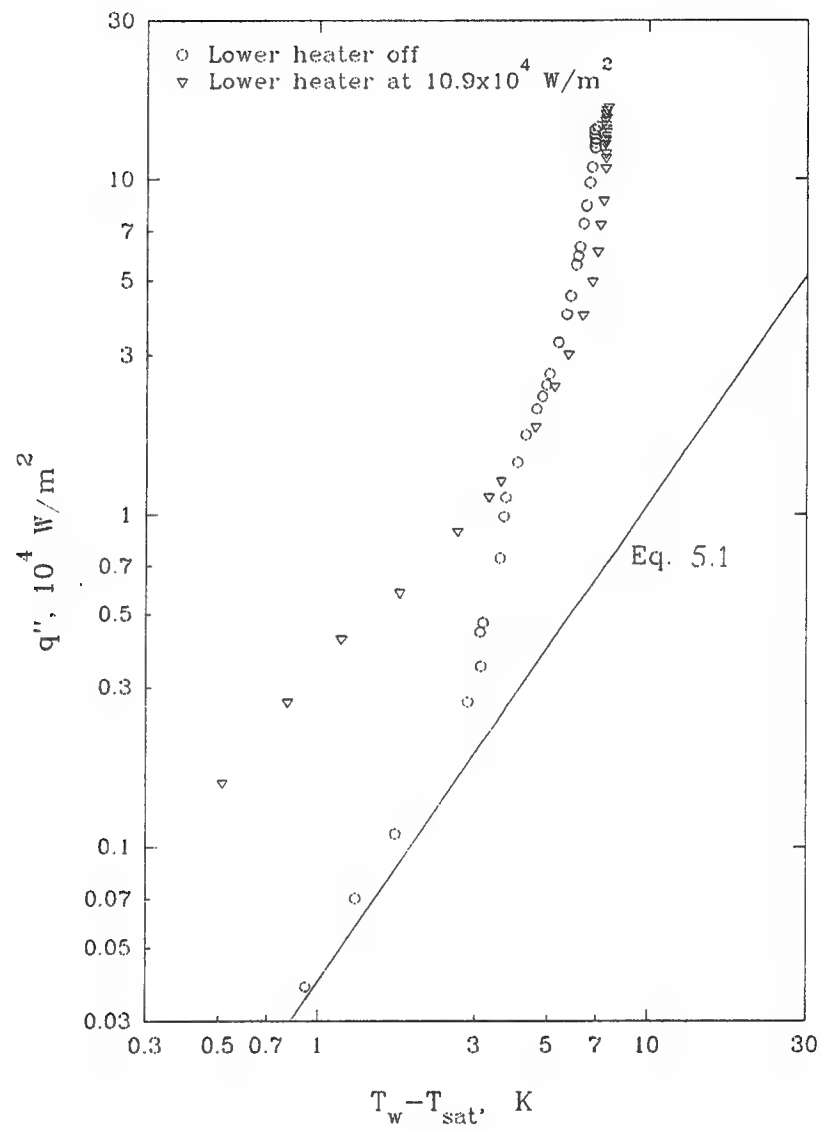


Figure 5.4 Effect of Lower Heater on Heat Transfer from an Upper Heater.

batch of wire, all the thermocouples read within $\pm 0.1\text{K}$ when immersed in liquid nitrogen. Therefore, for superheat, this is a better representation of the error than the former value.

The temperature T_w was extrapolated using the heater thermocouple reading and the heat flux (based on one-dimensional conduction model). Based on the uncertainties in thermal conductivity, heat flux, and heater thickness, the extrapolation uncertainty is about $\pm 5\%$. However, the calculated temperature drop along the thickness of the heater never exceeds 1 K. This gives the maximum uncertainty in extrapolation as $\pm 0.05\text{K}$. The maximum uncertainty in superheat ($T_w - T_{\text{sat}}$) then comes to $\pm 0.25\text{K}$.

In the CHF region, the power increments to the heater were decreased to $2.5 \times 10^3 \text{ W/m}^2$. Thus, the uncertainty in CHF is equal to this value plus the uncertainty in heat flux estimate. This gives a total uncertainty of less than 5% of the CHF.

The heat transfer coefficient h is the ratio of the heat flux and the superheat. The error in h is therefore dependent on the superheat and the uncertainty in heat flux measurement. The maximum relative error in h can then be written as: $0.03 + 0.25/(T_w - T_{\text{sat}})$.

5.3 Results and Discussion

Preliminary results revealed two important differences between the boiling curves of heaters in an array and solitary heaters. First, for the upper heaters in an array, the critical heat flux increased as the heat fluxes of the lower heaters increased. Secondly, the coefficient of heat transfer, h , during the preboiling regime increased dramatically as the heat flux to the lower heaters rose. The heaters not directly below a heater were not seen to have any significant effect on heat transfer characteristics. The heater just below the one under study was always the most influential. When any top heater in the array was studied with both of the lower heaters operating at a particular heat flux, the heat transfer characteristics were not significantly different from those with the lowest heater off. Hence, the following discussion involves only the effect of one heater operating below the heater under study. The experimental set-up thus allowed for four inter-heater distances and two heater lengths using both vertical orientations of the array.

Figure 5.4 shows the pool boiling characteristics of a heater with and without a lower heater operating at a fixed heat flux. A little bit of temperature overshoot - typical of highly wetting fluids like LN2 - is seen for the solitary heater case. As seen from the figure, the pre-boiling heat transfer coefficient was as much as 700% higher when the lower heater was in

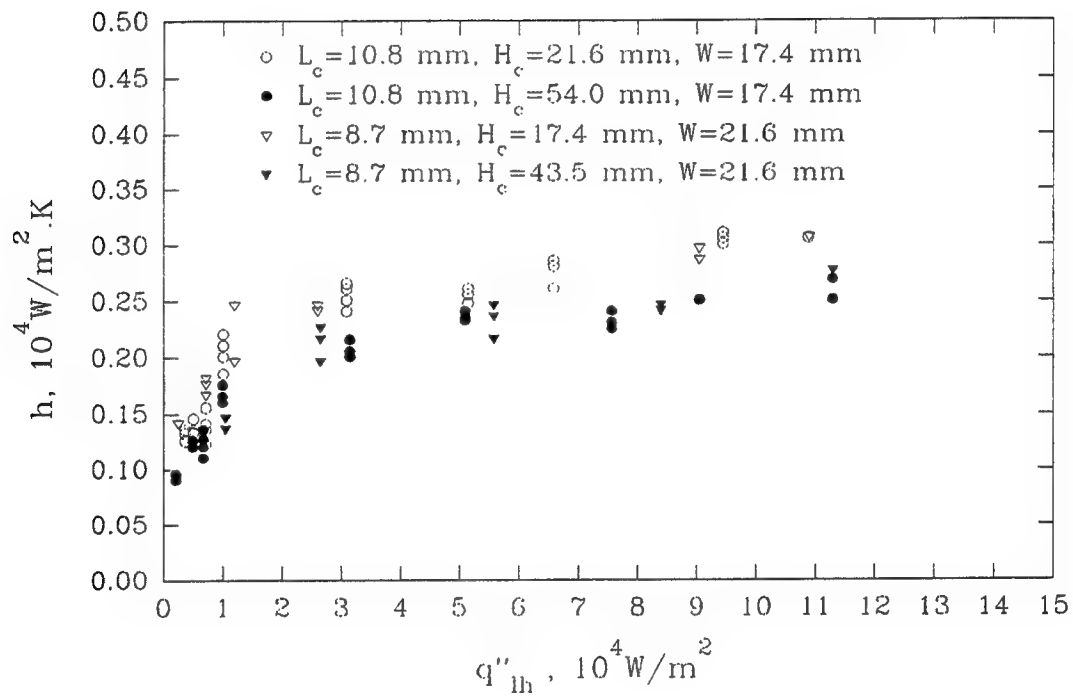


Figure 5.5 Effect of Lower Heater on Preboiling h .

operation. Similarly, the CHF was also enhanced from $1.44 \times 10^5 \text{ W/m}^2$ to $1.64 \times 10^5 \text{ W/m}^2$. The nucleate boiling portion of the curves are quite close. The curve with the lower heater on shifts a little bit to the right due to a slight suppression in nucleate boiling caused by the higher velocity flow. But this shift in nucleate boiling curve is not very pronounced. Hence, this study concentrated on characterizing the enhancement in the pre-boiling regime and the CHF.

The influence of the lower heater on the heat transfer coefficient prior to the onset of nucleate boiling is very pronounced. This is due to the intense convection caused by the bubble flow from the lower heater. Figure 5.5 shows the effect of the lower heater heat flux, q''_{lh} , on the pre-boiling heat transfer coefficient of the upper heater. As the heat flux to the lower heater increases, the value of h increases very rapidly, however, past $2.5 \times 10^4 \text{ W/m}^2$, increasing heat flux from the lower heater causes small increase in the heat transfer coefficient. Also, the enhancement in h decreases as the distance between the upper and lower heater is increased.

The heat transfer in the pre-boiling regime is due to mixed convection, the bubble-flow induced convection is assisted by natural convection. Hence, the heat transfer correlation for this regime has to incorporate both of these contributions.

$$\begin{aligned}
 Nu_{n,c} &= \alpha Ra_c^{*\delta} \\
 \text{where} \\
 \alpha &= 0.906 \left[1 + \frac{0.0111}{(W/W_\infty)^{3.965}} \right]^{0.2745} \\
 \delta &= 0.184 \left[1 + \frac{2.64 \times 10^{-5}}{(W/W_\infty)^{9.248}} \right]^{-0.0362} \\
 W_\infty &= 70 \text{ mm}
 \end{aligned} \tag{5.1}$$

Numerous correlations for natural convection from a finite vertical plate exist [43]. The best match was found to be the correlation of Park and Bergles [44], shown here as Equation 5.1. Although Equation 5.1 was proposed for small vertical heaters in R-113 (Freon-113), and the Ra_c^* in the present study exceeded the range of this correlation, it had a reasonable agreement with the LN2 data, as shown in Figure 5.4.

For a surface under mixed convection conditions, Churchill [45] correlated the mean Nusselt number at center of the surface using the equation

A similar approach was used in the present study. The natural convection Nusselt number was

$$Nu_c = [Nu_{n,c}^3 + Nu_{f,c}^3]^{1/3} \quad (5.2)$$

estimated using Equation 5.1, however, the forced convection Nusselt number poses a problem. The flow velocity due to the bubbles is difficult to obtain analytically. Hence, an empirical approach had to be used. Incropera et al.[46] proposed a general correlation, Equation 5.3, for small-flush heaters under forced convection. The value of C and p vary depending on heater geometry and fluid.

$$Nu_{f,c} = C Re_{L_c}^p Pr^{0.38} (\mu_o / \mu_h)^{9.11} \quad (5.3)$$

This equation (Equation 5.3) requires a knowledge of the Reynolds number. One way to obtain this information is through the measurement of fluid velocity due to the bubble flow. This, however, was not possible because the presence of large number of bubbles interferes with optical measurement techniques. Another way of obtaining the fluid velocity is by relating it to the vapor velocity, v_g .

The fluid velocity due to the bubble pumped flow can be assumed to be function of the vapor velocity and some fluid properties. With this assumption, we can write the fluid velocity over the heater as Equation 5.4. The first term in Equation 5.4 represents the vapor velocity

$$v_f = C_1 \left(\frac{q_{lh}''}{\rho_g h_{fg}} \right) \left(\frac{H_c}{W_l} \right)^n \quad (5.4)$$

from the lower heater. The second term can be termed as dissipation factor; this represents the effect on vapor velocity as the bubble source is moved lower. This effect takes place due to the lateral spread of bubble flow as it moves up in a liquid. The constant C_1 and exponent n in Equation 5.4 depend on the fluid properties and therefore have to be determined empirically. Equation 5.3 and 5.4 can be combined and written as Equation 5.5. The constants C_1 and C are

$$Nu_{f,c} = C_2 \left[\frac{\rho_f \left(\frac{q_{lh}''}{\rho_g h_{fg}} \right) \left(\frac{H_c}{W_l} \right)^n L_c}{\mu_f} \right]^p Pr^{0.38} \quad (5.5)$$

combined into C_2 and the last term in Equation 5.3 is dropped as it approaches unity for saturated liquid. A best fit correlation to the data was obtained. The best fit values of C_2 , n and p were: $C_2=21.50$, $n=-0.62$ and $p=0.24$. Combining equations 5.1, 5.2 and 5.5 we can write

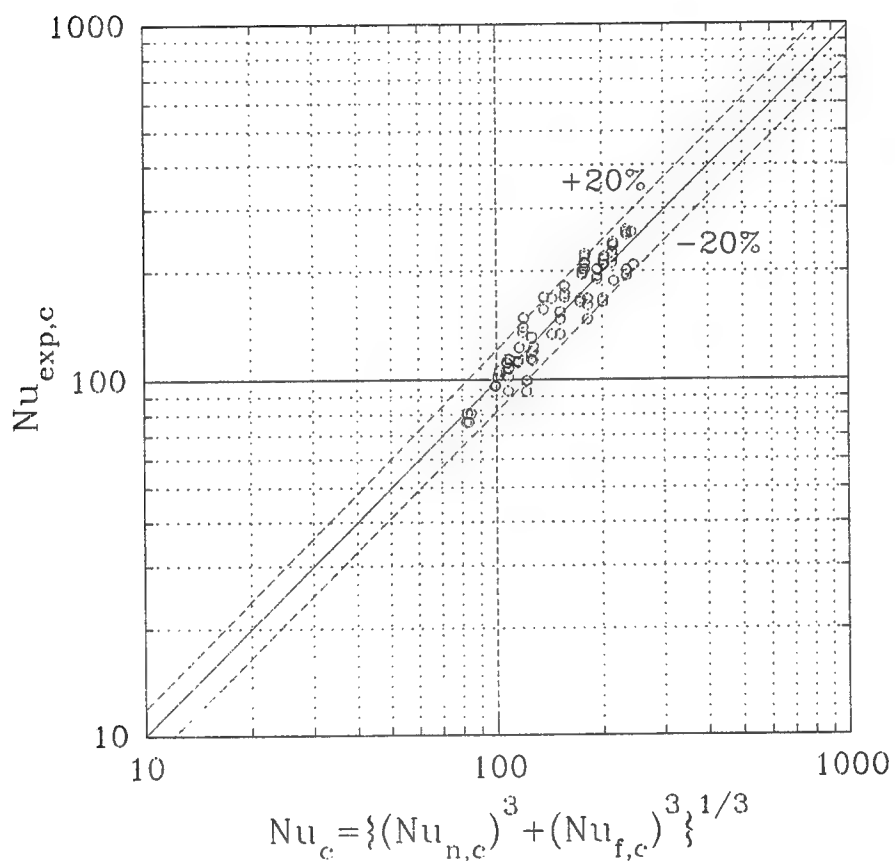


Figure 5.6 Preboiling h Correlation.

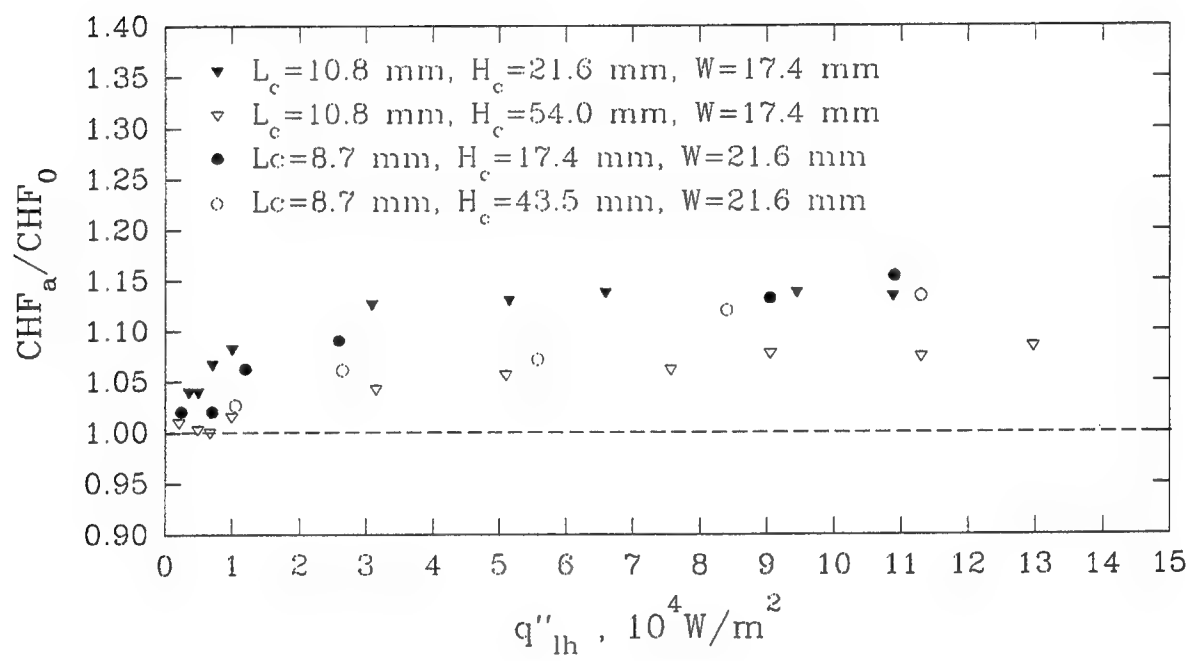


Figure 5.7 Effect of Lower Heater on CHF.

$$\begin{aligned}
 CHF_0 &= 0.9 CHF_{Zuber} \\
 \text{for} \quad L' &= \frac{L}{\sqrt{\frac{\sigma}{g(\rho_f - \rho_g)}}} > 6.0 \\
 \text{where} \quad CHF_{Zuber} &= 0.131 \rho_g h_{fg} \left[\frac{\sigma(\rho_f - \rho_g)g}{\rho_g^2} \right]^{1/4}
 \end{aligned} \tag{5.7}$$

the overall Nusselt number at the midpoint of the heater surface as Equation 5.6.

$$\begin{aligned}
 Nu_c^3 &= (\alpha Ra_c^{*b})^3 \\
 &+ \left(21.5 \left[\frac{\rho_f \left(\frac{q_{lh}''}{\rho_g h_{fg}} \right) \left(\frac{H_c}{W_l} \right)^{-0.62} L_c}{\mu_f} \right]^{0.24} Pr^{0.38} \right)^3
 \end{aligned} \tag{5.6}$$

Figure 5.6 shows the comparison of Equation 5.6 with the experimental data. As seen from the figure, most of the data fall within $\pm 20\%$ of the correlation. Although this is a significant spread, it can be explained by the fact that the experimental error in the preboiling regime can be fairly large due to the very low values of $T_w - T_{sat}$. The uncertainty in temperature difference was about 0.25 K; at a surface superheat of 1 K, this translates into a 25% error in $T_w - T_{sat}$ and a 28% error in h . Therefore, the correlation shows a reasonable fit to the data considering the experimental error.

The other point of interest in this study was the CHF region. As mentioned earlier, the flow caused by the lower heater elevates the CHF from the upper heater. Figure 5.7 shows the effect of lower heater heat flux on the CHF, here CHF_a/CHF_0 represents the ratio of CHF with the lower heater on to the CHF for the solitary heater. As shown in the figure, the CHF shows an increase as the heat flux from the lower heater is increased. When the heat flux from the lower heater rises higher than about $3.0 \times 10^4 \text{ W/m}^2$, increasing the heat flux of the lower heater causes lesser increase in CHF. Overall, the maximum enhancement due to the presence of the lower heater was around 15%. This enhancement also reduced as the distance between the lower and the upper heater increased. The values for critical heat flux from a solitary heater were

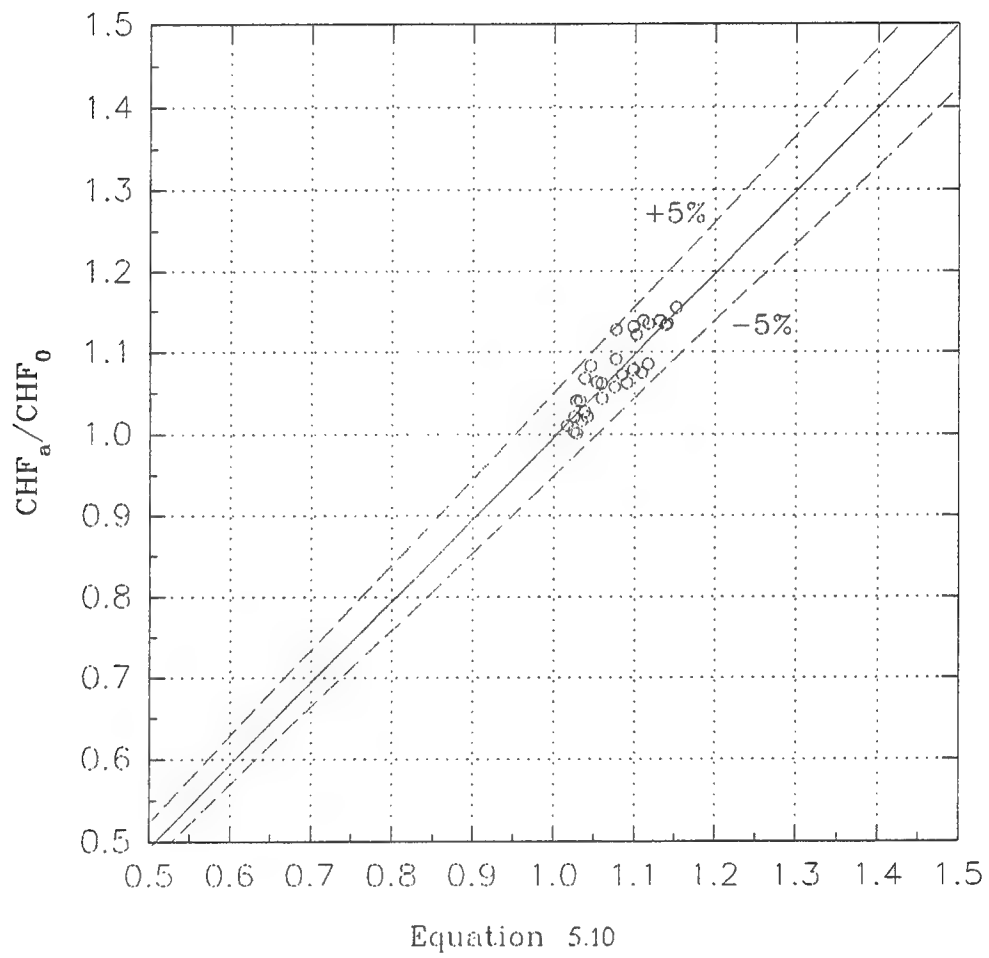


Figure 5.8 CHF Correlation Comparison.

found to correspond almost exactly with the asymptotic value from Lienhard and Dhir's correlation, Equation 5.7 [47] (note that the heater dimensions in this study exceeded the very small heater limit of $L' < 6.0$).

The CHF in flow boiling conditions generally correlates well to the Weber number of the flow [48]. Hence we can write the CHF ratio as Equation 5.8.

$$\frac{CHF_a}{CHF_0} = 1 + C_2 We_L^r \quad (5.8)$$

Using a similar approach to that used in writing the Reynolds number, the Weber number can be written as Equation 5.9. Then by combining Equations 5.8 and 5.9 we can write Equation 5.10 for the CHF ratio. The constant C_4 and r again depend on fluid properties and were

$$We_L = \left[\frac{\rho_f \left[C_1 \left(\frac{q_{lh}''}{\rho_g h_{fg}} \right) \left(\frac{H_c}{W_l} \right)^{-0.62} \right]^2 L}{\sigma} \right] \quad (5.9)$$

determined by a best fit of the data. The best fit value of C_4 was 0.08 and that of r was 0.24.

$$\frac{CHF_a}{CHF_0} = 1 + C_4 \left[\frac{\rho_f \left[\left(\frac{q_{lh}''}{\rho_g h_{fg}} \right) \left(\frac{H_c}{W_l} \right)^{-0.62} \right]^2 L}{\sigma} \right]^r \quad (5.10)$$

Figure 5.8 shows the comparison of the correlation with the data. As shown in the figure, the data fit the correlation to within $\pm 5\%$.

6. CONCLUSIONS AND FUTURE PLANS

Spray cooling is not a well understood process. The purpose of this study was to obtain design correlations for the heat flux and the CHF for LN2 spray cooling. This study used experimental heat transfer data reported in the previous report [22] and spray parameter data obtained during this study to obtain correlations for LN2 spray cooling process.

As part of this study, experiments were conducted to observe the effect of surface roughness. The rougher surfaces provided significantly higher heat transfer rates. This was attributed to the significant contribution of surface nucleate boiling for rougher surfaces. The smoothest surface had negligible surface nucleation. Secondary nucleation was identified as the most important contribution in spray cooling in the absence of surface nucleation. When surface nucleation is present it quickly becomes the overwhelming contributor.

The CHF was deemed to be caused by the choking of liquid replenishment to the surface by the vapor bubbles generated in the liquid film. A general empirical correlation was obtained for CHF; the correlation showed good agreement to previous data for water and R113 (although the data for R113 was not used in obtaining the correlation). The Weber number based on the spray velocity and surface hydraulic diameter was found to be the main parameter influencing the CHF. A correlation was also developed for the heat flux in LN2 spray cooling. However, a general correlation for spray cooling heat flux could not be obtained due to lack of pertinent data for other liquids.

The spray droplet velocity was identified as the most important parameter for both heat flux and CHF. The correlations showed good agreement with the experimental data. In conclusion, this study provided significant insight into the spray cooling mechanism and the important parameters involved. The study also succeeded in obtaining a general empirical correlation for CHF from horizontal surfaces which was heretofore unavailable. This correlation should prove to be a very useful design tool.

The second part of the study dealt with pool boiling from a vertical heater array. The presence of lower heaters increases both the critical heat flux and the preboiling heat transfer coefficient from the upper heater. Only the closest operating lower heater was found to have significant effect on the heat transfer characteristics of the upper heater. CHF was enhanced by as much as 15%; h , by as much as 700% when a lower heater was operating at some fixed heat

flux. This enhancement is attributed to the forced convection caused by the vapor generated from the lower heater. The amount of enhancement generally decreased as the distance between the lower heater and upper heater increased. A correlation based on mixed convection was found for the enhancement of heat transfer coefficient. This correlation gives the overall Nusselt number in terms of the natural convection Nusselt number and a forced convection Nusselt number (derived from the vapor flux from lower heater). Another correlation relating the enhancement in CHF to the Weber number was also obtained. Both of the above-mentioned correlations fit the data reasonably well.

Based on this study, it can be seen that in saturated pool boiling, the heat transfer from upper heaters is not degraded due to the vapor flow from the lower heaters. In fact, the effect is beneficial to the upper heaters. However, when a limited space exists in front of the heater array (as in a channel), this effect could indeed be detrimental due to insufficient space for vapor-escape/liquid-replenishment. There would be an optimum spacing in that case, beyond which the channel gap should not be reduced. This parameter is of great interest in electronic cooling and is currently being studied in more detail.

Future plans include obtaining the operating characteristics of power MOSFETs under spray cooling and pool boiling conditions. This is intended to demonstrate the capabilities of these heat transfer techniques in thermal management of high power electronics. The pool boiling study dealing with the influence of confined space on heat transfer from heater arrays is in progress. The study of liquid nitrogen flow boiling is also under way. The experimental set-up is currently being fabricated.

7. REFERENCES

- 1 Nisenhoff, M., "Superconducting electronics: current status and future prospects," *Cryogenics*, Vol. 28, No. 1, 1988, pp. 47-56.
- 2 Van Duzer, T., "Superconductor-semiconductor hybrid devices, circuits and systems," *Cryogenics*, Vol. 28, No. 8, 1988, pp.527-531.
- 3 Tucker, J. R., "Quantum limited detection in tunnel junction mixers," *IEEE Journal of Quantum Electronics*, Vol. QE-15, 1979, pp. 1234-1258.
- 4 McGrath, W. R., Raisanen, A. V., Richards, P. L., Harris, R. E., and Lloyd, F. L., "Accurate noise measurements of superconducting quasiparticle array mixers," *IEEE Trans. on Magnetics*, Vol. MAG-21, 1985, pp. 212-221.
- 5 Fox R. M., and Jaeger R. C., "MOSFET behavior and circuit considerations for analog applications at 77 K," *IEEE Trans. on Electron Devices*, Special Issue on Low Temperature Semiconductor Electronics, Vol. ED-34, No. 1, 1987, pp. 114-123.
- 6 Mueller, O., "Cryogenic power conversion: combining HT superconductors and semiconductors," AIP Conference proceedings 251, 1991, pp. 746-759.
- 7 Touloukian, Y. S., Powell, R. W., Ho, C. Y. and Clemens, P. G., *Thermophysical Properties of Matter The TPRC Data Series*, Vol. 1 & 2, IFI/Plenum, NY, 1970.
- 8 O'Conner, L., "High -Temperature Superconducting Motors," *Mechanical Engineering*, Vol. 116, No. 4, 1994, pp. 32.
- 9 O'Conner, L., "Building Natural Gas Locomotives," *Mechanical Engineering*, Vol. 116, No. 4, 1994, pp. 82-84.

- 10 Clarke, J., "Superconducting quantum interference devices for low frequency measurements, superconducting applications," *SQUIDS and Machines*, edited by Schwartz, B. R., and Foner, S., Plenum Press, NY, 1977, pp. 67-124.
- 11 Lavine, A. S., and Bai, C., "An analysis of heat transfer in Josephson junction devices," *J. of Heat Transfer*, Vol. 113, 1991, pp. 535-543.
- 12 Zuber, N., "On the Stability of Boiling Heat Transfer," *J of Heat Transfer*, Vol. 80, 1958, pp. 711-720.
- 13 Toda, S., "A study of mist cooling. 2nd. Report: Theory of mist cooling and its fundamental experiments," *Heat Transfer Japanese Research*, Vol. 3, No. 1, 1974, pp. 1-44.
- 14 Bonacina, C., Comini, G. and Del Giudice, D., "Evaporation of atomized liquids on hot surfaces," *Letters in Heat & Mass Transfer*, Vol. 2, 1975, pp. 401-406.
- 15 Tilton, D. E., "Spray Cooling," PH.D. Dissertation, University of Kentucky, Lexington, KY, 1989.
- 16 Pais, M. R., Chow, L. C., and Mahefkey, E. T., "Surface roughness and its effects on the heat transfer mechanism in spray cooling," *J. of Heat Transfer*, Vol. 114, 1992, pp. 211-219.
- 17 Sehmbey, M. S., Pais, M. R. and Chow, L. C., "A study of diamond laminated surfaces in evaporative spray cooling," *Thin Solid Films*, Vol. 212, 1992, pp. 25-29.
- 18 Yang, J., Chow, L. C., Pais, M. R., and Ito, A., "Liquid film thickness and topography determination using Fresnel diffraction and holography," *J. of Experimental Heat Transfer*, Vol. 5, 1992, pp. 239-252.

- 19 Sehmbey, M. S., Pais, M. R., and Chow, L. C., "Effect of surface material properties and surface characteristics in evaporative spray cooling," *J. of Thermophysics & Heat Transfer*, Vol. 6, No. 3, 1992, pp. 505-512.
- 20 Yang, J., Pais, M. R., and Chow, L. C., "Critical heat-flux limits in secondary gas atomized liquid spray cooling," *J. of Experimental Heat Transfer*, Vol. 6, No. 1, 1993, pp.55-67.
- 21 Lefebvre, A. H., *Atomization and Sprays*, Hemisphere, NY, 1989, Ch. 6.
- 22 Chow, L. C., Sehmbey, M. S., Lu, W. F., Pais, M. R., and Hahn, O. J. "Fundamental Studies in Blow-Down and Cryogenic Cooling," Wright Laboratory Interim Report No. WL-TR-93-2128, 1993.
- 23 Cooper, M. G., and Lloyd, J. P., "Transient local heat flux in nucleate boiling," Proc. 3rd. Int. Heat Transfer Conf., Chicago, Vol. 3, 1966, pp. 193-203.
- 24 Mesler, R., "A mechanism supported by extensive experimental evidence to explain high heat fluxes observed during nucleate boiling," *AIChE Journal*, Vol. 22, No. 2, 1976, pp. 246-252.
- 25 Mesler, R., and Bellows, W. S., "Explosive boiling: A chain reaction involving secondary nucleation," ASME Proc. of 1988 National Heat Transfer Conf., HTD-96, Vol. 2, 1988, pp. 487-491.
- 26 Mesler, R. B., "Improving nucleate boiling using secondary nucleation," *Pool and External Flow Boiling*, V. K Dhir & A. E. Bergles, Editors, ASME Press, 1992, pp. 43-47.
- 27 Rohsenow, W. M., "Boiling," *Handbook of Heat Transfer Fundamentals*, Rohsenow, W. M., Hartnett, J. P., and Ganić, E. N., Editors, 2nd. Ed., McGraw Hill, Inc., NY,

1985, Ch. 12.

- 28 M. Monde, "Critical heat flux in the saturated forced convection boiling on a heated disk with impinging droplets," *Heat Transfer - Japanese Research*, Vol. 8, No. 2, 1979, pp. 54-64.
- 29 M. Monde, "Critical heat flux in saturated forced convection boiling on a heated disk with an impinging jet," *J. Heat Transfer*, Vol. 109, 1987, pp. 991-996.
- 30 Y. Haramura and Y. Katto, "A new hydrodynamic model of critical heat flux applicable widely to both pool and forced convection boiling on submerged bodies in saturated liquids," *Int. J. of Heat & Mass Transfer*, Vol. 26, 1983, pp. 389-399.
- 31 Y. Katto, "Critical heat flux in forced convection flow," Proc. of ASME-JSME Thermal Engineering Conf., Vol. 3, 1983, pp. 1-10.
- 32 C.S.K. Cho and K. Wu, "Comparison of burnout characteristics in jet impingement cooling and spray cooling," National Heat Transfer Conference, Houston, HTD-Vol. 96, 1988, pp. 561-567.
- 33 M. Ghodbane and J.P. Holman, "Experimental study of spray cooling with Freon-113," *Int. J. Heat Mass Transfer*, Vol. 34, No. 4/5, 1991, pp. 1163-1174.
- 34 Mirza, S., "The behavior of Liquid Nitrogen from Aluminum Surfaces," *Int. Comm. Heat Mass Transfer*, Vol. 17, 1990, pp. 9-18.
- 35 Tuzla, K., Çökmez-Tuzla, A.F., Crowley, A.J. and Chen, J.C., "Cooling of Electronic Chips in Liquid Nitrogen," Proceedings of the Ninth Int. Heat Transfer Conf., Jerusalem, Israel, Heat Transfer, Vol. 2, Editor: G. Hetsroni, 1990, pp. 301-306.
- 36 Mudawar, I. and Anderson, T.M., "High Flux Electronic Cooling by Means of Pool

- Boiling - Part I: Parametric Investigation of the Effects of Coolant Variation, Pressurization, Subcooling, and Surface Augmentation." 1989 National Heat Transfer Conf., Heat Transfer in Electronics, HTD-Vol. 111, 1989, pp. 25-34.
- 37 Bergles, A.E., and Bar-Cohen, A., "Direct Liquid Cooling of Microelectronic Components," *Advances in Thermal Modeling of Electronic Components and Systems*, Vol. 2, Editors: Avram Bar-Cohen, and A.D. Kraus, ASME Press, NY, 1990, Ch. 5.
 - 38 McGillis, W.R., Carey, V.P., and Strom, B.D., "Geometry Effects on Critical Heat Flux for Subcooled Convective Boiling From an Array of Heated Elements," *J of Heat Transfer*, Vol. 113, 1991, pp. 464-471.
 - 39 McGillis, W.R. and Carey V.P., "Subcooled Convective Boiling of Binary Mixtures over an Array of Heated Elements," *J of Thermophysics and Heat Transfer*, Vol. 7, No. 2, 1993, pp 346-351.
 - 40 Gersey, C.O. and Mudawar, I., "Orientation Effects on Critical Heat Flux from Discrete, In-Line Heat Sources in a Flow Channel," *J of Heat Transfer*, Vol. 115, 1993, pp. 973-985.
 - 41 You, S.M., Simon, T.W., and Bar-Cohen, A., "Pool Boiling Heat Transfer with an Array of Flush-Mounted, Square Heaters," *Topics in Heat Transfer*, HTD-Vol. 206-2, ASME, 1992, pp. 63-72.
 - 42 Polentini, M.S., Ramadhyani, S., and Incropera, F.P., "Two-Phase Thermosyphon Cooling of an Array of Discrete Heat Sources in a Rectangular Cavity," *Advances in Electronic Packaging*, EEP-Vol. 4-2, ASME, 1993, pp. 899-908.
 - 43 Krane, R. J., Bar-Cohen, A., Jaeger, R. C., and Gaensslen, F. H., "MOS Electronics and Thermal Control for Cryogenically-Cooled Computer Systems," *Advances in Thermal Modeling of Electronic Components and Systems*, Vol. 2, Ed. Avram Bar-Cohen and

Allan D. Kraus, ASME Press, NY, 1990, Ch. 4.

- 44 Park, K.-A. and Bergles, A.E., "Natural Convection Heat Transfer Characteristics of Simulated Microelectronic Chips," *J. Heat Transfer*, Vol. 109, 1987, pp. 90-96.
- 45 Churchill, S.W., "A Comprehensive Correlation Equation for Laminar Assisting Forced and Free Convection," *AIChE J.*, Vol.23, 1977, pp. 10-16.
- 46 Incropera, F.P, Kerby, J., Moffatt, D.F. and Ramadhayani, S., "Convection Heat Transfer from Discrete Heat Sources in a Rectangular Channel, *Intl. J. Heat and Mass Transfer*, Vol. 29, 1986, pp. 1051-1058.
- 47 Lienhard, J.H. and Dhir, V.K, "Hydrodynamic Prediction of Pool-Boiling Heat Fluxes From Finite Bodies," *J. Heat Transfer*, Vol. 95, 1973, pp. 152-158.
- 48 Mudawwar, I.A. and Maddox, D.E., "Critical Heat Flux in Sub-Cooled Flow Boiling of Fluorocarbon Liquid on a Simulated Electronic Chip in a Vertical Rectangular Channel," *Intl. J. Heat and Mass Transfer*, Vol. 32, 1989, pp. 379-394.